UNIVERSITY OF APPLIED SCIENCE

WEIHENSTEPHAN-TRIESDORF

Faculty of Forestry

Bachelor-Thesis

Oxygen consumption and production measured by high-resolution respirometry in leaf preparations from *Robinia pseudoacacia*

Author: **Rebecka Alheit Hardorp, 1364112**

Supervisors: **Prof. PhD Jörg Ewald**

Ao.Univ.-Prof. PhD Thomas Roach

Ao.Univ.-Prof.i.R., PhD Erich Gnaiger

Place, submission date: **Weihenstephan, 2024-01-15**

Erklärung bzgl. der Zugänglichkeit von Diplom-/Bachelor-/Masterarbeiten

Verfasserin

Name, Vorname **Hardorp, Rebecka Alheit**

Betreuer

Name, Vorname **Ewald, Jörg**

Thema der Arbeit **Oxygen consumption and production measured by high-resolution respirometry in leaf preparations from *Robinia pseudoacacia***

Ich bin damit einverstanden, dass die von mir angefertigte Arbeit mit o.g. Titel innerhalb des Bibliothekssystems der Hochschule Weihenstephan-Triesdorf aufgestellt und damit einer breiteren Öffentlichkeit zugänglich gemacht wird. Die Arbeit darf im Bibliothekskatalog der Hochschule Weihenstephan-Triesdorf (und zugeordneten Verbundkatalogen) nachgewiesen werden und steht allen Nutzern der Bibliothek entsprechend den jeweils gültigen Nutzungsmodalitäten der Hochschulbibliothek der HSWT zur Verfügung. Ich bin mir auch darüber im Klaren, dass die Arbeit damit von Dritten ohne mein Wissen kopiert werden kann.

Die Veröffentlichung der Arbeit habe ich mit meinem Betreuer und falls zutreffend, mit der Firma/Institution abgesprochen, die eine Mitbetreuung übernommen hatte.

☐ Ja

☐ Ja, nach Abschluss des Prüfungsverfahrens am _____

☐ Ja, nach Ablauf einer Sperrfrist von_____Jahren

☐ Nein

Ort Datum Unterschrift Verfasserin

Als Betreuer bin ich mit der Aufnahme im Bibliothekssystem der Hochschule Weihenstephan-Triesdorf einverstanden.

Ort Datum Unterschrift Betreuer

I want to thank in particular:

Thanks to my mother, who supported me with much love throughout my studies.

I would like to thank my children Emma and Mio for their understanding that I often did not have time for them.

Many thanks to Thomas Roach for his great support.

Big thanks to Erich Gnaiger for his extraordinary willingness to mentor me. The analysis and interpretation of the oxygen kinetics would have been impossible without his guidance.

Many thanks to the whole Oroboros team.

'Imagination is more important than knowledge. For knowledge is limited to all we now know and understand, while imagination embraces the entire world, and all there ever will be to know and understand.' – Albert Einstein

Table of contents

Abbreviations

ADP	adenosine diphosphate
Ama	antimycin A
AOX	alternative oxidases
As	ascorbate
ATP	adenosine triphosphate
Azd	azide
Chl	chlorophyll
Chl-a	chlorophyll-a
BL	blue light
c	cytochrome *c*
CI	consumption-irradiance
c_{O_2}	oxygen concentration
Ctl	catalase
Dig	digitonin
ETS	electron transfer system
F_V/F_m	maximum quantum efficiency
IBG	instrumental background
J_D	dark oxygen consumption
J_L	light-induced oxygen consumption
KCN	cyanide
L	light intensity
lh	leaf homogenate
LHC	light-harvesting complexes
M	malate
$NADP^+$	nicotinamide adenine dinucleotide phosphate
$O_2^{-\bullet}$	superoxide radical

$^1O_2$	reactive singlet oxygen
$OH^{\bullet}$	hydroxyl radical
OXPHOS	oxidative phosphorylation
P	pyruvate
PB	PhotoBiology
PFD	photon flux density
PI	photosynthesis-irradiance
POS	polarographic oxygen sensor
PSII	photosystem II
PUMP	plant uncoupling mitochondrial proteins
q_E	high-energy quenching
q_P	photochemical reaction
RL	red light
ROS	reactive oxygen species
Rot	rotenone
Rox	residual oxygen consumption
S	succinate
SHAM	salicylic acid hydroxamate
TCA	tricarboxylic acid
Toc	α-Tocopherol
WL	white light

1 Introduction

Air pollution and the changing climate pose significant threats to the well-being and functionality of forest ecosystems, profoundly endangering their ecological, economic, and service-related functions. The impacts of rising temperatures and extreme weather events - such as droughts, storms, temperature fluctuations, and precipitation - on the health of trees are often intricately intertwined with the effects of pollution, including nitrogen deposition and tropospheric ozone levels. These pollutants can exhibit synergistic effects, making it challenging to isolate their individual impacts. For instance, the continuous decline in foliar phosphorus concentrations in Europe, leading to reduced tree growth, can be attributed in part to the combined influences of forest soil acidification, atmospheric nitrogen deposition, and climate change. This complex interplay underscores the difficulty of disentangling the specific contributions of various stressors to observed ecological changes.

In navigating this intricate web of interactions, the use of indicators becomes indispensable in modern forest ecophysiological research. Indicators play a fundamental role in helping researchers to unravel the nuanced relationships between trees and diverse stress-inducing factors. They also aid in providing more accurate estimates of the extent of damage imposed on trees and entire forest ecosystems. In essence, the development and use of indicators is pivotal for gaining a deeper understanding of the multifaceted challenges faced by forests in the context of contemporary environmental pressures (Potočić, 2023).

Stress in plants, caused by adverse external conditions, results in a range of responses, including altered gene expression, cellular metabolism, and changes in growth rates and crop yields. Stress can be categorized into abiotic (physical or chemical) and biotic (biological, such as diseases or insects). Stress-tolerant plants undergo acclimation to specific stressors over time. Severe stresses may lead to metabolic dysfunctions, preventing flowering and seed formation, ultimately causing plant death (Gull *et al.*, 2019).

Especially trees face various natural and anthropogenic stresses in their environment, necessitating resilience and resistance mechanisms against biotic and abiotic challenges, which are crucial for the survival of long-lived tree species. As trees persist in the same location for many decades or even centuries, they must acclimate their growth and reproduction to continually changing atmospheric and pedospheric conditions. The importance of understanding how different stress factors influence the physiological responses of forest trees becomes particularly relevant in the context of climate change (Polle and Rennenberg, 2019).

It is therefore important to find early indicators in easily accessible compartments of the tree. Leaves are an obvious target, especially since they are responsible for the energy supply and sites of high metabolic activity.

In leaves, oxygen plays a critical role in five fundamental ecophysiological processes:

(1) In the presence of sunlight, chlorophyll and other pigments in the chloroplasts absorb light energy. This energy is used to convert carbon dioxide and water into glucose, the primary product, and oxygen, a waste product. Plastids are bioenergetic organelles which are responsible for photosynthesis and many metabolic activities (Maliga, 2014). Under the influence of light, chloroplasts develop through reorganization of the original proplastids and turn green in many cases due to the formation of chlorophyll. A fully grown mesophyll cell in the leaf contains 50 to 100 chloroplasts which align themselves according to the distribution of light in the cell. In the chloroplast, three different spaces are connected to the electron transfer system (ETS): the intermembrane space, the stromal space, and the thylakoid lumen. The latter is arranged in so-called grana stacks and connected by tubes.

During photosynthesis the absorption of light occurs primarily through the special molecular arrangement of chlorophyll (Chl) and carotenoids within the light-harvesting complexes. The photon energy is absorbed by the pigment, (e.g. Chl), which excites an electron into a higher energetic state. Two main excitation states are referred to as the first and second singlet states, which are attributed to different rotation and vibration states. The return to the fundamental state proceeds in various ways: In addition to photochemistry, energy is released via fluorescence and heat, restoring the energy level of the pigment back to the ground state.

The photosynthesis complexes in the thylakoid membrane cause the oxidation of water and the reduction of nicotinamide adenine dinucleotide phosphate ($NADP^+$). The resulting potential difference uses the two absorbed photons to transfer electrons from the water to $NADP^+$. In addition, the light energy is used to pump protons into the lumen of the thylakoids via the cytochrome *b6f* complex. This leads to a proton gradient between the lumen and the stroma. The energy obtained is also used for the biosynthesis of adenosine triphosphate (ATP) (Piechulla and Heldt, 2023). A low pH of the thylakoid lumen slows down electron flow through the cytochrome *b6f* complex, as well as regulating the release of excess-absorbed light energy as heat (Roach and Krieger-Liszkay, 2019), as described below.

(2) During photosynthesis, the effect of light also involves photorespiration. Therefore, the measurement of photosynthetic oxygen production is the sum of total photosynthesis

diminished by photorespiration and residual oxygen consumption (*Rox)* defined as the oxygen consumption due to oxidative side reactions remaining after inhibition of the mitochondrial and chloroplast electron transfer pathways to oxygen (Gnaiger, 2020). Net and gross photosynthesis can be distinguished by the direct measurement of net photosynthesis and correction for light-enhanced dark respiration to obtain gross photosynthesis (Shimakawa, Kohara and Miyake, 2021; Went *et al.,* 2022).

Photosynthesis in plants takes place in the chloroplasts, and cellular respiration primarily in the mitochondria. These two processes are interconnected and maintain a balance in the oxygen and carbon dioxide levels within the plant and the environment. The mitochondrial and photosynthetic ETS are similar. In both cases enzymatic complexes are coupled to one another by a proton gradient (Taylor, 2019).

(3) In terms of oxygen and glucose metabolism, respiration is the reverse of the photosynthesis reaction and serves to produce ATP. In this process, oxygen is consumed as it reacts with glucose. This energy is then utilized for various metabolic activities, including growth, maintenance, and reproduction. The mitochondrial respiratory ETS supports vital processes in plant cells similar to animal cells. The respiratory ETS is localized in the mitochondria, the cell's powerhouse. In the plant respiratory ETS, organic compounds derived from glucose are converted in the tricarboxylic acid (TCA) cycle into redox equivalents and by oxidative phosphorylation (OXPHOS) into ATP, which is used for energy transformation to support the biosynthesis of metabolic intermediates. These features make this machinery central to various biological functions, including cell proliferation, differentiation, and adaptation to stress. Because mitochondria are thought to receive commands and provide signals to control biological outcomes, alterations in mitochondrial metabolism may occur due to changes in nuclear gene expression. However, if a cell engages in a process such as proliferation or differentiation without adequately functioning mitochondria, the cell is likely to experience a metabolic crisis, potentially leading to senescence and cell death. In this scenario, properly functioning mitochondria can be viewed as an early checkpoint before cells commit to developmental or stress response processes. A notable example occurs within the first few minutes of the plant life cycle, where mitochondria are fully active almost immediately after seed rehydration. However, plants are unlikely to begin their life cycle with poorly functioning mitochondria (Barreto *et al.*, 2022).

'Recent themes in plant mitochondrial research include linking mitochondrial composition to environmental stress responses, and how this oxidative stress impacts on the plant

mitochondrial function. Similarly, interest in the signalling capacity of mitochondria, the role of reactive oxygen species (ROS), and retrograde and anterograde signalling has revealed the transcriptional changes of stress responsive genes as a framework to define specific signals emanating to and from the mitochondrion' (Taylor, 2019).' The ability to withstand stress is a complex trait. Besides other cell organelles, plant mitochondria play a particularly important role in stress tolerance (Taylor, 2019).

(4) Oxygen plays a third role in the context of oxidative stress. Oxidative stress leads to oxidative damage by ROS. ROS production is a component of *Rox*. ROS are formed when compounds of the respiratory and photosynthetic ETS are highly reduced, and the membrane potential is high. Superoxide radical ($O_2^{-\bullet}$), hydrogen peroxide (H_2O_2) and the hydroxyl radical ($OH^{\bullet}$) are collectively referred to as ROS and may have a necrotic damaging effect on cells. On the other hand, ROS serve important signaling functions, including in eustress and acclimation (Roach *et al.*, 2018, 2023). Environmental influences, temperature extremes, nutrient deficiencies and high light intensities cause stress and can increase ROS production (Piechulla and Heldt, 2023). Leaf senescence can be partly attributed to ROS. 'Under stress, increased production of ROS and associated signalling activates senescence' (Shimakawa, Krieger-Liszkay and Roach, 2022).' To minimize oxidative stress, various antioxidant mechanisms of plants serve to neutralize ROS and limit their harmful effects. These mechanisms include antioxidants such as glutathione, ascorbic acid, α-tocopherol, and enzymes including superoxide dismutase, catalase, and glutathione peroxidase. Increasing photosynthetically active photon flux density (PFD) leads to an increase in the protein content of the detoxifying enzymes (Shimakawa, Krieger-Liszkay and Roach, 2022).

ROS production caused by high light intensity contributes to the degradation of the chloroplasts and is responsible for the breakdown of starch. This leads to the disruption of the carbohydrate balance mechanism during the light-dark cycle, which regulates the starch accumulation respectively degradation (Piechulla and Heldt, 2023).

The natural protective mechanisms, such as short-term acclimation, are no longer sufficient to protect photosynthesis when light absorption is increased above a threshold. If too much light is absorbed, the downstream processes can no longer be used for the photochemical reaction (q_P). The outflow of excess energy and its deletion in photosystem II (PSII) occurs largely at the expense of maximum quantum efficiency (F_V/F_m) in the form of heat (Y[NO]) (Klughammer and Schreiber, 2008). Excess energy can also be released from the light-harvesting complexes (LHC). This high-energy quenching (q_E) is regulated via the

transthylakoidal pH difference. If the light energy cannot be dissipated via q_E, the chlorophyll molecules can enter the long-lived triplet state that reacts with ground-state oxygen to produce the highly reactive singlet oxygen ($^1O_2$). Damage caused by $^1O_2$ can be prevented by specific carotenoids, such as zeaxanthin, and α-tocopherol, but their antioxidant capacity is limited. If the photo-oxidative damage of PSII predominates, this process leads to photoinhibition. Moreover, ROS formed by the reduction of photosynthetic efficiency induces photo-oxidation, which is responsible for the destruction of proteins, membrane lipids and chloroplast components, among others (Schmitz, 2011; Roach, 2022).

(5) In plant debris (e.g. fallen leaves), light-induced oxidative damage and structural damage by freezing-thawing cycles lead to photodecomposition. Enhancement of the processes of degradation by light is referred to as photodegradation or photodecomposition and is thought to play a significant role in carbon cycling by modifying the bioavailability of stored energy in dead plant material for further decomposition by microbiota (Wang *et al.*, 2021; Hussain *et al.*, 2023). If all photosynthesizing and mitochondrial elements are no longer functional, oxygen-consuming processes are entirely *Rox* including photodegradation. This can be demonstrated by the absence of any effects of specific inhibitors of the mitochondrial (Gnaiger, 2020) and chloroplast electron transfer pathways on oxygen consumption (Piechulla and Heldt, 2023).

If the binding ground state or the anti-bonding energy state cannot be used photochemically (q_P) or with high-energy quenching (q_E), oxidations will take place (molecules find the most energetically favourable position on the potential curve at zero) (Laisk and Oja, 2018). Therefore, potentially, photodecomposition can be quantified by measurement of light-induced oxygen consumption which became the most innovative aspect of the present study.

To understand the nutrient release of plant mass loss, the mechanisms of photodegradation play an important role in decomposition cycling. Photodegradation is a process in litter decay, involving the photochemical mineralization of complex macromolecules (e.g., lignin) absorbing solar radiation. This results in the breakdown of organic matter into smaller components, furthermore in wet conditions. Solar radiation indirectly affects microbial activity through photofacilitation, transforming recalcitrant compounds into labile organic matter. Because mass loss starts with the senescence of leaves the processes of photodegradation and senescence intersect and influence each other in the cycle of plant leaves.

Photodecomposition or photodegradation is the result of chemical reactions where the chemical structure is broken down by photons and cause the transformation of the bonds of a chemical.

During the photochemical process an atom or molecule absorbs a quantum of light energy from a photon and tends to form a new structure or get a combination with other molecules and transfers excitation energy (protons and electrons) which causes a chemical chain reaction. The major degradation pathways and the products that are formed happen in the presence of oxygen through photochemical and free radical reactions (Ruban, 2016; Hussain *et al.*, 2023). A better understanding is required of how (sun)light can accelerate the decomposition process of plant material during the photochemical mineralization and photofacilitation. Photodegradation plays a big role in forest ecosystems and there is a need to examine its chemical interactions (breaking down complex molecules) with decomposer organisms (interact with the products of photodegradation) to obtain better estimations of how carbon cycling might be affected by climate change. The so-called photofacilitation effect makes cell-wall compounds bioavailable for microbial activity and enhances the action of extracellular enzymes. Complex macromolecules like lignin are able to absorb solar radiation (Pieristè *et al.*, 2019). Light and oxygen play an important role during the chlorophyll degradation which is accompanied by intermediate and final (photo)products. In aqueous media with chlorophyll the light induced products are hydroxy-pheophytin *a*, pheophytin *a* and hydroxy-lactone-pheophytin *a* (Petrović, Zvezdanović and Marković, 2017).

All five roles of oxygen can be assessed quantitatively by respirometry. A high level of destruction of the leaf material is expected to result from crude homogenization performed in preparation of leaves for respirometric measurements. Respirometry is the quantitative measurement of oxygen consumption, i.e. the measurement of a very slow oxidative process (combustion). The combination of respirometry and calorimetry played an essential role in bioenergetics (Gnaiger, 1983). This offers an indirect calorimetric approach by measuring oxygen uptake and converting the consumed oxygen into an enthalpy change using the oxycaloric equivalent. Liebig showed that the substrates of oxidative respiration were proteins, carbohydrates, and fats (Liebig, 1842). These chemical changes in living cells are called metabolism. The contributions of carbohydrate and fat to metabolism can be quantified by the respiratory quotient, the amount of carbon dioxide produced in comparison with the amount of oxygen consumed at the same time. The intake of oxygen (external respiration) alone does not trigger the metabolism; rather, the activity of metabolism (internal respiration) regulates breathing (Lusk, 1928).

In respirometry the ETS-linked oxygen consumption is distinguished from *Rox*. *Rox* arises from lingering oxidative side reactions of the electron transfer pathway in mitochondrial preparations

or living cells. Various conditions with inhibition of respiration, referred to as ROX states, allow for the measurement of residual oxygen consumption (Gnaiger, 2020).

In the Oroboros mitochondrial research laboratory in Innsbruck, a wide variety of mammalian cells are used for respirometric measurements. Beyond mammalian cells, Oroboros collaborates with the research group 'Stress Metabolism' from the Department of Botany, University of Innsbruck, which conducts research on algae. The project 'ALAS - Acclimation strategies of algae to changing light intensity' led by Prof. Thomas Roach carries out measurements with the O2k (*ALAS – Universität Innsbruck*, no date). To my knowledge, no measurements have been carried out with the Oroboros O2k on plant leaves to date. That was the decisive impulse for selecting the topic of the present study.

The Oroboros O2k is a high-resolution respirometer that allows to study the mitochondrial physiology of mammalian cells. This technology enabled crucial new insights into bioenergetics, mitochondrial physiology, and the diagnosis of mitochondrial diseases (Gnaiger *et al.*, 2020). However, this does not exclude the use of other cell forms in aqueous suspensions, such as algae. The development of the PhotoBiology (PB) Module extended the application of the O2k to photosynthesis and other photochemical processes. This is demonstrated by several publications, where the essential interplay of bioenergetics between mitochondria and chloroplasts is pivotal in maintaining metabolic balance and governing metabolite generation for the purpose of growth and cell concentration regulation (Went *et al.*, 2022; Vera-Vives, Perin and Morosinotto, 2022).

For the measurement of the dynamics of complex coupled metabolic pathways of mitochondria with the O2k, the sample type is the object of a respirometric experiment, which is defined by the specifications of the population and by a specific sample preparation. This includes tissue homogenates (*Sample type*, no date). These measurements provide insights into the mitochondrial stress response processes. Mitochondrial dysfunction in plants can manifest itself in various ways and lead to various physiological and molecular changes. These include changes in energy metabolism, disruptions in the respiratory ETS with increased ROS production, altered mitochondrial membrane potential and altered gene expression. The role of plant mitochondria is not limited to providing energy in the dark phase. They are of central importance for the ATP supply to the cytosol during photosynthesis in the light phase and fulfil special functions, such as the so-called overflow protection mechanisms. These involve alternative oxidases (AOX), which are insensitive to antimycin A (Ama) and cyanide (KCN) but can be inhibited by salicylic acid hydroxamate (SHAM). The AOX pathway is activated by

an excessive reduction of mitochondrial ubiquinone, which may be caused by an increase in pyruvate (P) concentration. AOX are not proton pumps and decrease the coupling efficiency by bypassing Complex IV. Furthermore, plant uncoupling mitochondrial proteins (PUMP) are membrane proteins which are soluble in water and in lipids. This allows them to penetrate the lipid phase of a membrane through diffusion in the protonated and unprotonated form. The electron transfer in the presence of uncouplers is stimulated even in the absence of adenosine diphosphate (ADP) (Piechulla and Heldt, 2023).

Diagnostically relevant conditions are established for measuring mitochondrial function and respiratory capacities in core energy metabolism. Standard respiratory coupling-control states are maintained under defined conditions. A concept-driven terminology of mitochondrial respiratory states ensures general applicability (Gnaiger *et al.*, 2020).

Mitochondrial LEAK respiration is defined as: 'The contribution of intrinsically uncoupled oxygen consumption is studied by preventing the stimulation of phosphorylation either in the absence of ADP or by inhibition of the phosphorylation pathway. The corresponding states are collectively classified as LEAK states when oxygen consumption compensates mainly for ion leaks, including the proton leak' (Gnaiger *et al.*, 2020).'

Mitochondrial OXPHOS capacity is defined as: 'The ET- and phosphorylation pathways comprise coupled segments of the OXPHOS-system and provide reference values of respiratory capacities. The OXPHOS capacity is measured at kinetically saturating concentrations of ADP, inorganic phosphate, fuel substrates and oxygen' (Gnaiger *et al.*, 2020).'

Mitochondrial ET capacity is defined as: 'Compared to OXPHOS capacity, the oxidative ET capacity reveals the limitation of OXPHOS capacity mediated by the phosphorylation pathway. By application of external uncouplers, ET capacity is measured as noncoupled respiration' (Gnaiger *et al.*, 2020).'

1.1 Aim and significance for forestry

The aim of the present study is to characterize the light-induced oxygen consumption (J_L) and production of a leaf homogenate with the O2k. The focus is placed not only on chloroplasts and photosynthesis but particularly on mitochondrial respiration and non-mitochondrial oxygen consumption. The information gained from respirometry may serve as early indicators of checkpoints in the life cycle of the plant.

In the context of forestry, respirometric measurements with the O2k could become part of regular tree monitoring. In addition to other methods, respirometry provides a tool for elucidating the trees' response mechanisms and strategies to combat biological and abiotic stress. Furthermore, the condition and activity of mitochondria in leaves can serve as an indicator of environmental conditions and stresses and potentially add another aspect to a better understanding of the effects of climate change on trees (Barreto *et al.*, 2022). Altered mitochondrial activity and non-mitochondrial oxygen consumption could indicate specific physiological and environmental conditions or structural alterations on the level of the cells and organelles of the leaves (Schwarzländer and Finkemeier, 2013). This knowledge can help to take timely measures in the context of forest management.

Considering that the trend in hours of sunshine increased linearly by 10 percent between 1951 and 2022 (*Deutscher Wetterdienst*, no date), the influence of changing light conditions on forests and ecosystems in general is significant. The knowledge of photodegradation in litter decay contributes to a more comprehensive understanding of forest ecosystems (Hussain *et al.*, 2023). This understanding, in turn, can help to optimize sustainable forest practices, resource management, and ecosystem conservation efforts within the forestry industry.

2 Materials and methods

2.1 Sample collection

For sample collection an approximately ten-meter high *Robinia pseudoacacia* tree was chosen close to the Oroboros laboratory (Figure 1 and 2). Leaves were always taken from the same branch in the lower part of the tree. The green (non-senescent) and yellow (senescent) leaves were immediately processed for sample preparation (Figure 3). In addition, a branch with green leaves was removed from the test tree and dried openly in a large beaker at room temperature 24 hours before homogenization (Figure 4).

Figure 1: The test tree *Robinia pseudoacacia* in front of the Oroboros laboratory.

Figure 2: Freshly picked *Robinia pseudoacacia* leaf.

2.2 Preparation of cut leaf pieces

To cut a fresh leaf into small pieces is a way of sample preparation to measure photosynthetic activity during irradiation. The leaf tissue is injured at the interface, but the main population of cells remains intact.

First, the main leaf vein in the middle was removed with a pair of scissors and a tweezer because vascular tissue likely responds differently and can exert a confounding effect on measurements. Second, it was divided into approximately five mm^2 sections.

2.3 Preparation of leaf homogenate

A leaf homogenate refers to a sample consisting of a homogenized mixture of mostly damaged cells and cell components from plant leaves. The process of homogenization involves destroying the cell structure to extract the intracellular organelles and components such as proteins, enzymes, metabolites, and other molecules using a liquid medium, comparable to mammalian tissue homogenates (Meszaros *et al.*, 2022). During homogenization organelles such as mitochondria and chloroplast may remain intact, in which case a homogenate can be compared to mitochondrial or chloroplast isolations. During crude homogenization, however, the membranes of organelles may be damaged. In contrast, even entire living cells may remain intact, depending on the intensity of homogenization.

Two different media were chosen for the homogenization of leaves. The medium MiR05 is specifically designed for measurements with the Oroboros O2k and was the first choice (*MiR05-Kit*, no date). 4-(2-Hydroxyethyl)piperazine-1-ethanesulfonic acid (HEPES) is commonly used as a medium for cell culture (Pfanz and Heber, 1986). For this purpose, a 1 M HEPES (Sigma-Aldrich: H7523-250G) solution was prepared with pH 7.
All homogenates were prepared with the same leaf mass concentration. The optimum concentration was tested initially. 5 mL of medium were added to 50 ±1 mg of cut leaf pieces. For weighing, the leaf material was cut into pieces as described above. For this purpose, a Mettler Toledo XS205 analytical balance and a 5 mL Sartorius pipette were used. Using tweezers, the leaf parts were transferred into a homogenizing tube, filled with 5 mL of the appropriate medium and homogenized using the rotary piston at a speed of 600/min (Potter-Elvehjem-Homogenisator) (Figure 3). The homogenization process took about five minutes, and the tube was continuously cooled in an ice bath. After a minute of sedimentation, the supernatant was decanted into a labelled 15 mL Falcon tube. Subsamples of these homogenate stocks were placed into a -20 °C freezer or immediately used for measurements with the O2k.

Figure 3: Homogenization of the cut leaf pieces.

Figure 4: Air-dried branch after 24 h at room temperature in the laboratory.

2.4 Microscopy

A microscopic examination of the leaf homogenate was carried out using transmission light microscopy (Olympus BX50). As expected, most leaf cells were broken, although some intact cells could be found (Figure 6). After adding a 0.9 percent sodium chloride solution, the cell was observed to break open. Since the vacuole was still turgid, it can be assumed that the cell must still have been in an intact state. The lens-shaped chloroplasts appeared largely undamaged.

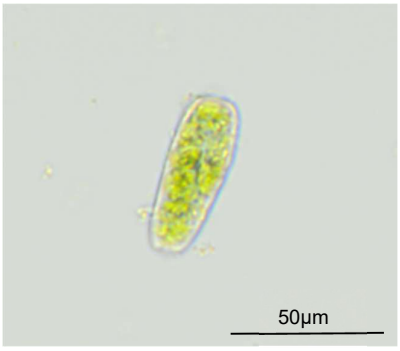

Figure 5: A cell of the leaf homogenate.

2.5 Spectrometry of chlorophyll content

Chlorophyll content of the homogenate was quantified via a spectrophotometer. A cryopreserved fresh green leaf homogenate and an air-dried leaf homogenate were measured with technical repeats of two. After an extraction in 80 % acetone absolute, the extinctions of the samples were measured at 663.6 and 646.6 nm. The extinction coefficients of chlorophyll a and b were calculated according to (Porra, Thompson and Kriedemann, 1989).

2.6 High-resolution respirometry

The Oroboros O2k allows high-resolution respirometric measurements of small amounts of biological samples for mitochondrial and cell research. Each O2k consists of two chambers (A and B) where the samples are added in aqueous suspension. Every chamber is connected to a polarographic oxygen sensor (POS) and includes a stirrer. During the measurements the chambers are closed with the stoppers which have a capillary for titrations and are calibrated to an exact chamber volume of 2 mL (Gnaiger *et al.*, 2023)

In addition to the basic version, there are additional modules for the O2k, such as the PB-Module which 'has been developed for conducting measurements of PhotoBiology (PB), including photosynthesis' (*PB-Module*, no date).'
The modular system is supported by DatLab 8, a software which records the measurements with the O2k. Different layout options can be selected for the visualisation of traces of different signals of the O2k and their time derivatives (*DatLab*, no date). The following signals are displayed in real-time as explained below.

Concentration c_{O_2} is the amount of elemental dissolved oxygen n_{O_2}, per volume of aqueous medium. The O_2 solubility in the aqueous medium relative to pure water is applied as the solubility factor F_M which is typically 0.89 to 0.92 in various culture and respiration media (Gnaiger, 2020).

Flux / Slope is the time derivative of the c_{O_2} corrected for instrumental oxygen background flux (see below). In an ideally closed chamber external fluxes are excluded; then the concentration changes depend on the internal chemical reactions. Then respiratory flux expressed per unit of chamber volume can be calculated from the negative slope of oxygen concentration over time (*Flux / Slope*, no date).The flux of photosynthetic oxygen production is calculated from the positive slope of oxygen concentration over time (Went *et al.*, 2022).

Flux, *J*, is flow (chemical flow or advancement of reaction per unit time) divided by the volume of the chamber or by various expressions of the amount of sample in the chamber (*Flux*, no date).

Light intensity, *L*, expressed in units of amount of photons per second per square meter [$\mu mol \cdot s^{-1} \cdot m^{-2}$] of blue (450 nm), red (610 nm) or white light (horticulture lighting) can be controlled accurately with the PB program (*PB Light Source*, no date).

Regular quality controls of the O2k ensure the accuracy of the measurement. Marks are set at selected time intervals of a plot. The following test are explained below.

A **stirrer test** provides a quick evaluation of the performance of the POS. After stopping and restarting the stirrer for a short period of time the increase of the oxygen signal should be rapid and monoexponential (*Stirrer test*, no date).

Air calibration (mark R1) is the routine step of the POS calibration before starting a respirometric experiment. The experimental aqueous medium is equilibrated at the partial pressure of oxygen in water-saturated air. It is performed in the partially opened chamber to allow a gas phase (air) to equilibrate with the aqueous phase (*Air calibration*, no date).

Zero calibration (mark R0) is the second step, after the air calibration, of the POS and may be performed as part of the instrumental background (IBG) test. After adding dithionite, the dissolved oxygen is fully consumed. Zero calibration is performed in the closed chamber (*Zero calibration*, no date).

In the **instrumental** O_2 **background** test (IBG) the changes of oxygen concentration over time (O_2 slope) are measured in the closed chamber in the absence of samples in the range of experimental oxygen levels. The IBG was monitored at three different oxygen levels (Figure 6). The linear IBG regression was calculated by DatLab from three marks set on the plot of the O_2 slope and expressing it as a function of the corresponding c_{O_2}. The background correction is based on the two parameters of the linear IBG regression, a^0 the extrapolated intercept at zero c_{O_2} and b^0 the linear IBG slope for statistical analysis of instrumental reproducibility as internal quality control in high-resolution respirometry (Baglivo *et al.*, 2022). In the example of Figure 6, a^0 was -2.7562 $pmol \cdot s^{-1} \cdot mL^{-1}$ and b^0 was 0.0213 $pmol \cdot s^{-1} \cdot mL^{-1}/\mu M$.

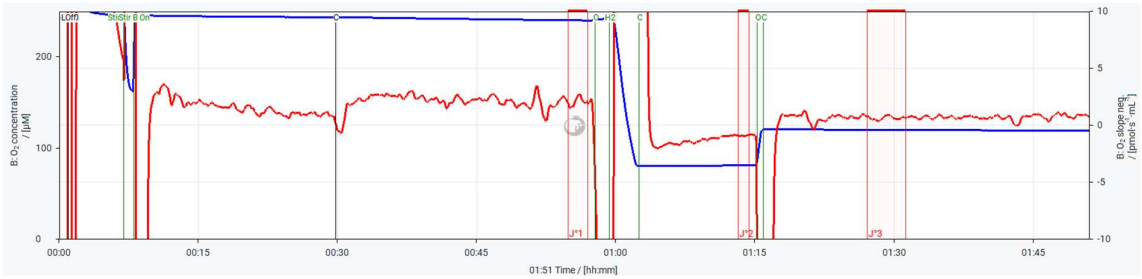

Figure 6: Instrumental O_2 background (IBG) test with three oxygen levels. Left axis: O_2 concentration [µM] (blue plot). Right axis: O_2 slope negative [pmol·s^{-1}·mL^{-1}] (red plot). Performed in MiR05 at 20 °C. Marks J°1, J°2, and J°3 were set on the plot of the O_2 slope negative. After performing a stirrer test and air calibration, the chamber was closed for monitoring the IBG at the first oxygen level near air saturation. For the second level H_2 was injected (event 'H2') to reach a c_{O_2} of approximately 80 µM. To obtain a third level the chamber was opened (event 'O') and closed (event C) for a short period.
Experiment: 2023-11-14_XA-002_08_IBG (chamber B).

For adding the sample, the stopper was removed from the chamber after air calibration, the stirrer was switched off, the appropriate volume of medium was removed with a Sartorius pipette and then filled up again with leaf homogenate. After this partial volume replacement, the stirrers were switched on, the chambers were closed again with the stoppers. Then an effective experimental volume of two mL was obtained with an additional volume of the suspension filling the stopper capillary. The event 'lh' was set with the information on the leaf homogenate and the pipetted volume. After the measurement relevant marks were set on the oxygraphy traces. The mark information (mark statistics) was exported to an excel file for further data analysis.

2.7 PB-Module and photosynthesis-irradiance curves

Switching the irradiance by the LEDs of the PB-Module on and off causes an intermittent disturbance of the oxygen signal. This is apparent as artificial increase of the oxygen slope after switching on the light and a symmetrical decrease of the oxygen slope after switching off the light (Figure 7A). For detailed analyses, the experimental traces of photosynthesis (based on the positive time derivative of c_{O_2}) are corrected for these effects induced by large changes of light intensity. Correspondingly, analyses of oxygen consumption (based on the negative time derivative of c_{O_2}) are corrected for the artificial decrease of the negative oxygen slope after switching on the light and a symmetrical increase of the negative oxygen slope after switching off the light (Figure 7B).

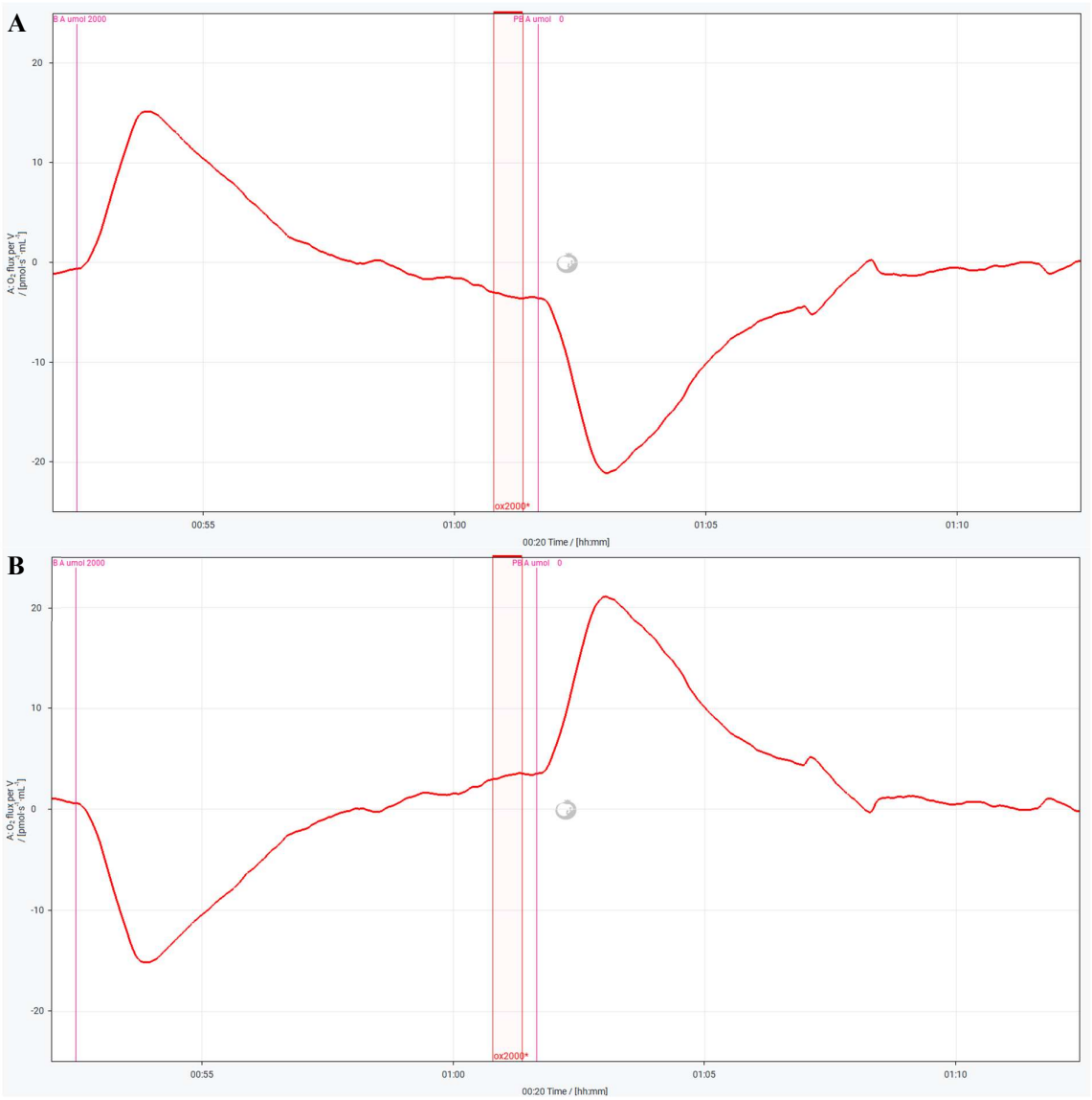

Figure 7: Disturbance of the oxygen flux after switching on and off the light at c_{O_2} of 260 µM. Based on the positive (**A**) or negative (**B**) time derivative of c_{O_2}. O_2 flux per V [pmol·s^{-1}·mL^{-1}] (chamber A). Performed in MiR05 at 20 °C. Experiment: 2023-11-23_XA-004_02_chl-a_vs_lh+chl-a, compare Figure 20.

The kinetic effect of light intensity on the flux of photosynthetic oxygen production is conventionally described in photosynthesis-irradiance (PI) curves (Figure 8).

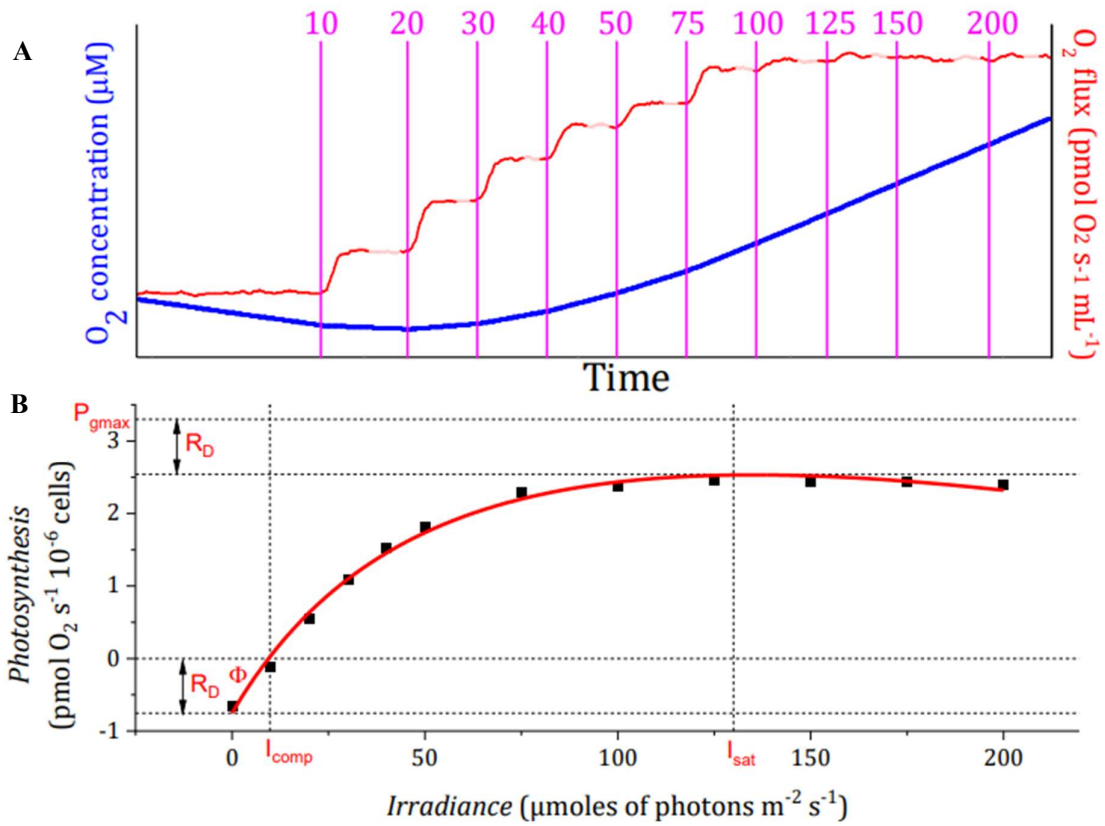

Figure 8: Construction of a PI curve. (**A**) The diagram shows one photosynthesis experiment of low-light-acclimated microalgae from Vera-Vives *et al*. (2022). The step-by-step increasing light intensities (pink vertical lines) induce an increasing O_2 flux (red plot) calculated from c_{O2} (blue plot). Light intensities up to 100 µmol·s^{-1}·m^{-2} increase the O_2 flux. (**B**) The PI curve shows the data from these experiments. The following abbreviations describe the curve: initial slope (Φ), compensation point (I_{comp}), rate of dark respiration (R_D), rate of maximal gross photosynthesis (P_{gmax}), saturation point (I_{sat}) (Vera-Vives, Perin and Morosinotto, 2022).

2.8 Definition of sample numbers

In the following text sample numbers refer to Table 1.

Sample Number	Preparation	Date of measurement	DatLab file
1	Fresh green leaf homogenate, cryopreserved	2023-11-07	2023-11-07_Q3-004_02_green_ctl.dld8
2	Fresh green leaf homogenate, cryopreserved	2023-11-07	2023-11-07_XA-004_04_green_O_C.dld8
3	Fresh green leaf homogenate, cryopreserved	2023-11-08	2023-11-08_Q3-004_02_azd.dld8
4	Fresh green leaf homogenate, cryopreserved	2023-11-10	2023-11-10_Q3-004_02_c_S_azd_nahco3.dld8
5	Fresh green leaf homogenate, cryopreserved	2023-11-23	2023-11-23_XA-004_02_chl-a_vs_lh+chl-a.dld8
6	Fresh green leaf homogenate, cryopreserved	2023-11-10	2023-11-23_Q3-004_02_bluelight_toc.dld8
7	Fresh green leaf homogenate, cryopreserved	2023-11-08	2023-11-08_XA-004_03_O2_P.dld8
8	Fresh green leaf homogenate, cryopreserved	2023-11-10	2023-11-10_XA-004_02_redlight.dld8
9	Fresh green leaf homogenate, cryopreserved	2023-11-10	2023-11-10_XA-002_03_O2kinetik_R0.dld8
10	Air-dried leaf homogenate, cryopreserved	2023-11-15	2023-11-15_XA-002_02_bluelight.dld8
11	Yellow leaf homogenate, cryopreserved	2023-11-23	2023-11-23_XA-002_03_yellowleaf_chl-a.dld8

Table 1: Sample catalogue.

3 Results

3.1 Dark respiration and photosynthetic oxygen production

To express the flux of photosynthetic oxygen production as a positive value, the stoichiometric number for oxygen is set at 1, such that an increase of the oxygen concentration in the closed O2k-chamber and hence a positive time derivative (slope) results in a positive oxygen flux (Gnaiger, 2020). A photosynthesis-irradiance curve (Figure 8) is shown in Figure 9 for an intact (non-homogenized) leaf cut into small pieces. Dark respiration is shown as a negative value. With increasing light intensity, the compensation point is reached, when the processes of oxygen consumption are first compensated and subsequently exceeded by photosynthetic oxygen production. Above the compensation point of increasing light intensity, net photosynthetic oxygen flux increases towards a plateau. But it may already decline over time at a high light intensity due to photoinhibition or depletion of CO_2. The latter possibility was excluded by the absence of an effect on oxygen consumption by addition of bicarbonate as will be shown later (Figure 15). After switching off the light, a peak of light-enhanced dark respiration is observed, and dark respiration approaches the steady state at an identical level of pre-irradiance dark respiration. The latter was 10.0 $pmol \cdot s^{-1} \cdot mL^{-1}$ which corresponds to 1.04 $pmol \cdot s^{-1} \cdot mg^{-1}$ at 19.2 mg fresh mass of the leaf sample in the 2 mL chamber.

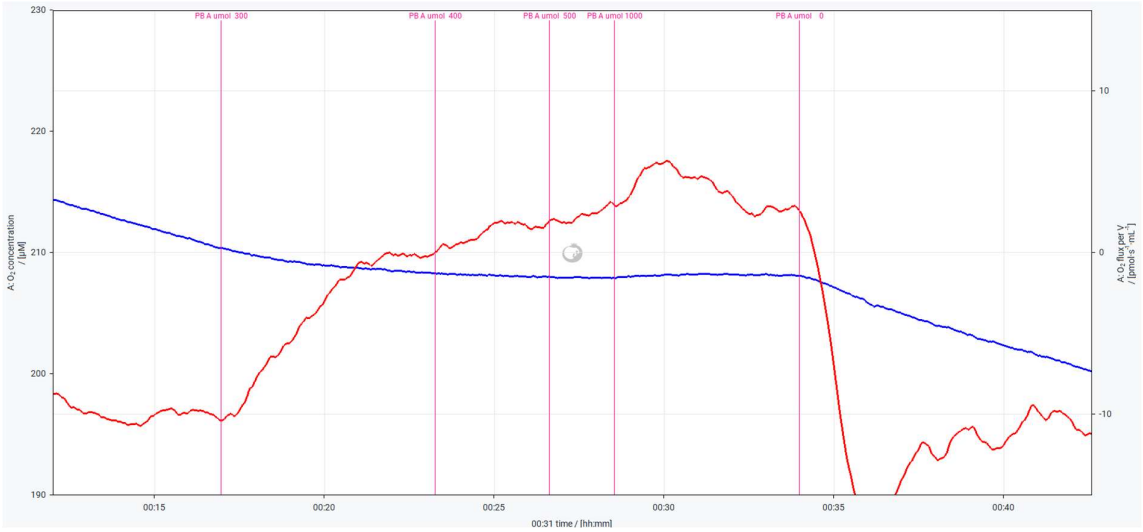

Figure 9: Dark respiration (negative) and photosynthesis (positive) in cut leaf pieces. Left axis: O_2 concentration [µM] (blue plot). Right axis: photosynthetic O_2 flux per V [$pmol \cdot s^{-1} \cdot mL^{-1}$] (red plot). At the beginning of the measurement the sample was added to MiR05 at 20 °C. Light intensities (300, 400, 500 and 1000 $\mu mol \cdot s^{-1} \cdot m^{-2}$) were chosen corresponding to a range of 10800 to 54000 lux. Experiment with 19.2 mg of cut leaf pieces. The plots are shown after a peroid of equilibration. Experiment: 2023-11-14_Q3-004_04_PS (chamber A).

3.2 Test experiments with leaf homogenates

Contrary to the original expectations, homogenates of leaves showed an increased rate of oxygen consumption immediately at the onset of irradiation (Figure 10). This indicates that photodegradation processes predominated any possibly remaining photosynthetic activity of leaf homogenates. In this case, it is more convenient to express the derivative of oxygen concentration over time as the negative slope by setting the stoichiometric number for oxygen at -1. Then light-induced oxygen consumption J_L is a positive value where the light intensity L is expressed in units of photons per second per square meter [µmol·s^{-1}·m^{-2}]. Dark oxygen consumption is J_D (at L=0). Preliminary experiments with fresh samples (data not shown) resulted in similar values of J_D measured in cryopreserved samples.

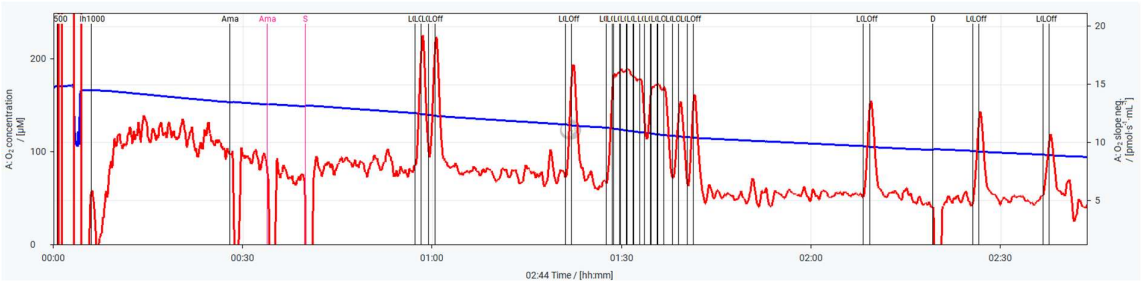

Figure 10: Dark oxygen consumption (J_D, positive) and light induced increase of oxygen consumption (J_L, positive) in leaf homogenate. Left axis: O_2 concentration [µM] (blue plot). Right axis: O_2 slope negative [pmol·s^{-1}·mL^{-1}] (red plot). At the beginning of the measurement the sample was added to MiR05 at 20 °C. During stabilization of J_D antimycin A was titrated in two steps, followed by succinate. J_L was controlled by repeated by 60 second intervals of internal illumination (vertical black lines, 'LOn' and 'LOff'). No effect of ADP. Experiment: 2023-10-13_Q3-004_02_Ama_S_D (chamber A).

3.3 Leaf homogenate dilutions

In order to obtain dark oxygen consumption J_D above the limit of detection of the O2k, different dilutions of fresh and cryopreserved leaf homogenate were initially tested (Figure 13). These test experiments revealed that a partial replacement of 1200 µL of pure respiration medium by the same volume of stock leaf homogenate (Section 2.3) corresponded to a suitable leaf fresh mass concentration of 10 mg/mL which was applied in all subsequent experiments.

3.4 The nature of oxygen consumption of leaf homogenates

To analyse the nature of dark oxygen consumption, several chemicals were applied to interrogate specific mitochondrial functions (Figure 11).

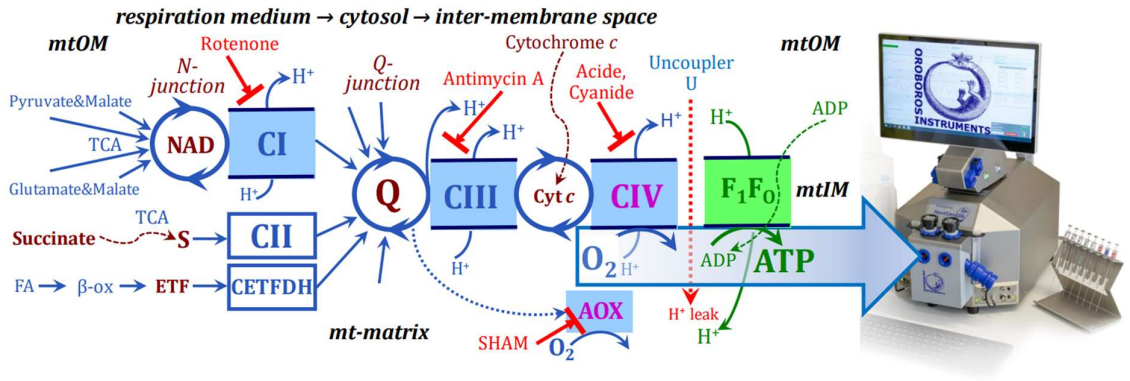

Figure 11: Mitochondrial electron transfer system. Symbolic representation of the mitochondrial electron transfer system (ETS) coupled to the phosphorylation system. mtIM and mtOM: mitochondrial inner and outer membrane. CI, CIII, and CIV: electron transfer Complexes I, III, and IV which are H^+ pumps. CII and CETFDH: Complex II and electron transferring flavoprotein dehydrogenase Complex which are not H^+ pumps. FA: fatty acids. β-ox: β-oxidation. TCA: tricarboxylic acid cycle. F_1F_O: ATP synthase. Dashed curved arrows: titrations into the respiration medium of compounds for which the intact plasma membrane is usually not permeable without permeabilization by digitonin. mt-matrix: mitochondrial matrix separated by the mtIM from the inter-membrane space. BJLked arrows: inhibitors for which the plasma membrane is permeable. NAD: NAD^+/NADH redox couple. Q: ETS-reactive coenzyme Q. Modified after ref. (Gnaiger, 2020).

These titrations were occasionally performed at different time points during an experiment when oxygen had not stabilized. Then the effect of the titrated substance cannot be evaluated by simple analysis of flux before and after the titration, but the undisrupted trend of the flux changing over time was evaluated (see Rotenone in Figure 13). The following ETS-linked pathway chemicals and their possible impact are described in ref. (*MitoPedia*, no date).

a) Pyruvate (P): P is a substrate used to stimulate the NADH-dependence pathway through Complex I. When 1 µL 2 mol/L P (Sigma-Aldrich: P2256) was added after 2.5 h incubation and varying light intensities dark oxygen consumption was not stimulated (Figure 12). Malate (M) was not added, which might explain the lack of stimulation if pyruvate-linked anaplerotic capacity is not expressed.

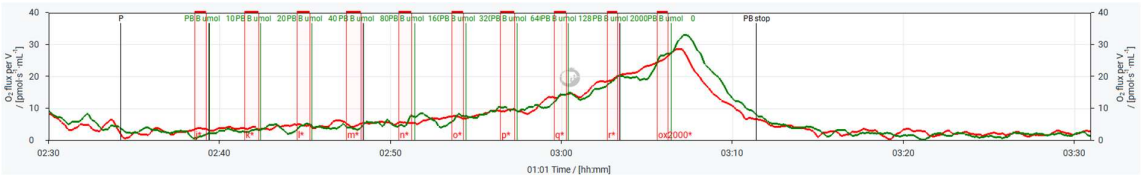

Figure 12: Oxygen flux as a function of time in the second PB-program (blue light). Overlay of red and green plots for chamber A and B, respectively. Both axis: O_2 flux per V [pmol·s^{-1}·mL^{-1}]. At the beginning of the measurement the sample was added to MiR05 at 20 °C. No effect of P on J_D. The PB-program is described in the Section 3.5. After the final 300 seconds of dark, the end of the PB-program is indicated (PB stop) and the measurement of J_D continued. The plots are shown after a period of previous measurement. Experiment: 2023-11-08_XA-004_03_O2_P.

b) Rotenone (Rot): Rot specifically blocks the transfer of electrons from NADH to ubiquinone in Complex I, leading to the inhibition of energy flow in mitochondria. The addition of 1 µL 1 mM Rot (Sigma-Aldrich: R8875) had no effect on the cryopreserved leaf homogenate (Figure 13).

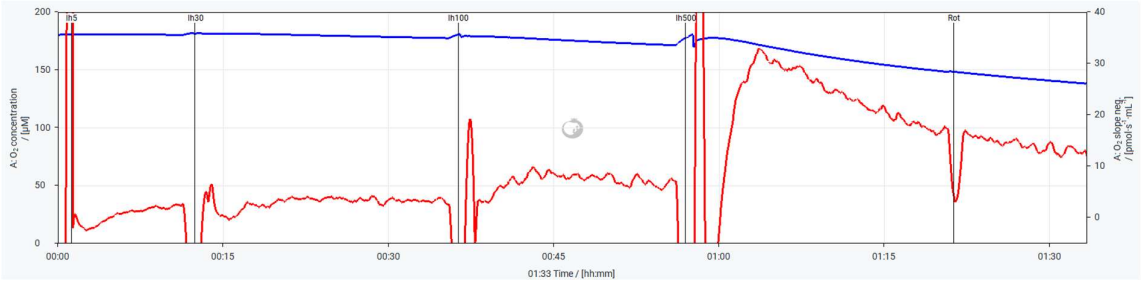

Figure 13: J_D after increasing partial volume replacements of leaf homogenate (5, 30, 100, and 500 µL). No effect of Rot added during the stabilization phase of J_D. For further explanation see Figure 9.
Experiment: 2023-10-04_Q3-004_02 (chamber A).

c) Succinate (S): In Figure 10 when 20 µL 1 M S (Sigma-Aldrich: S2378) was added after Rot the increased J_D might indicate the stimulation of LEAK-respiration. This is the mitochondrial oxygen consumption in the absence of ADP which mainly compensates for the proton leak across the mitochondrial inner membrane.

d) Adenosine diphosphate (ADP): In coupled mitochondria ADP stimulates respiration to the active state of oxidative phosphorylation (OXPHOS). However, ADP (10 µL 500 mM; Merck: 117105-1GM) was without any effect. This might be due to the intact plasma membrane prohibiting the transport of S to mitochondria (Figure 10).

e) Digitonin (Dig): This hypothesis was rejected by adding 1 µL 8.1 mM Dig (Sigma-Aldrich: D5628) to permeabilize the plasma membrane, which had no effect (Figure 14). In summary the data of Figure 5 indicate a non-mitochondrial nature of dark oxygen consumption.

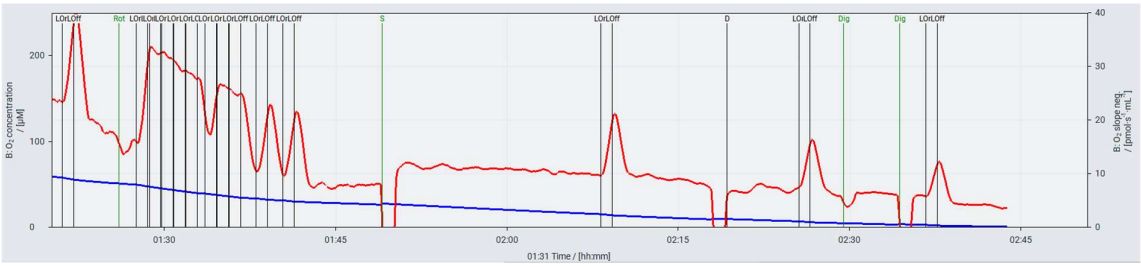

Figure 14: The effect of Rot on J_D and J_L using the internal illumination and stimulation of J_D by S. No effect of ADP and Dig. For further explanation see Figure 9. The plots are shown after a peroid of previuos measurement.
Experiment: 2023-10-13_Q3-004_02_Ama_S_D (chamber B).

f) Cytochrome *c* (c): A further experiment is required to test the possibility that homogenization caused the loss of c across the outer mitochondrial membrane if damaged by homogenization. In the presence of externally added c (5 µL 4 mM; Sigma-Aldrich: C7752), however, there was no stimulatory effect of S (Figure 15).

g) Antimycin A (Ama): Ama inhibits the transfer of electrons from ubiquinone to cytochrome c in Complex III. The result is impaired oxygen consumption in functional mitochondria. The addition of 1 µL 5 mM Ama (Sigma-Aldrich: A8674) to the cryopreserved

leaf homogenate apparently decreased J_D but a simple decline of J_D with time cannot be excluded which then would indicate no inhibitory effect of Ama (Figure 10). S, which was subsequently titrated, increased minimally the oxygen consumption. This cannot be explained by mitochondrial S-pathway function which depends on a functional Complex III. Likewise, the addition of ADP had no effect.

h) Azide (Azd) and cyanide (KCN): Like the Complex III inhibitor Ama the Complex IV inhibitors Azd (100 µL 4 M, Sigma-Aldrich: S2002) and KCN (4 µL 0.5 M, Sigma-Aldrich: 60178) had no inhibitory effect on dark oxygen consumption. Azd was added in the presence of c and S without causing any change of oxygen consumption (Figure 15). KCN paradoxically stimulated dark oxygen consumption when it was either added in the presence or absence of SHAM (Figure 16). Theoretically this could be explained by inhibition of catalase by KCN if H_2O_2 accumulated and thus reduced dark oxygen consumption which then would increase in the absence of dismutation of H_2O_2.

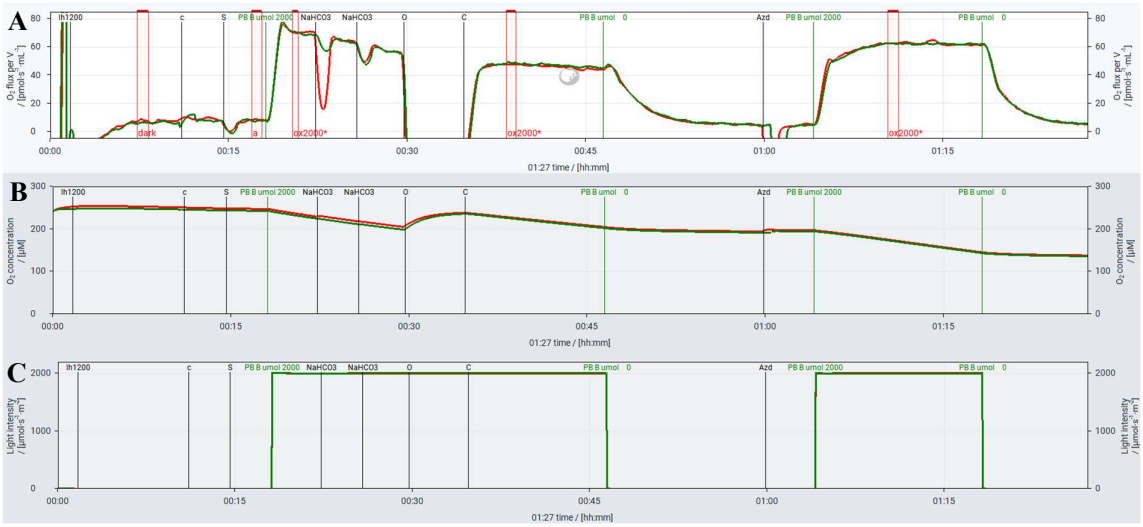

Figure 15: Effect of c and S on J_D and followed by J_L with NaHCO3 titrations and reoxygenation (O = open chamber; C = closed chamber). Overlay of red and green plots for chamber A and B, respectively. At the beginning of the measurement the sample was added to MiR05 at 20 °C. No effect of Azd on J_D, but increased J_L. (**A**) O_2 flux per V [pmol·s^{-1}·mL^{-1}], (**B**) oxygen concentration [µM], and (**C**) light intensity [µmol·s^{-1}·m^{-2}] plotted as a function of time.
Experiment: 2023-11-10_Q3-004_02_c_S_azd_nahco3.

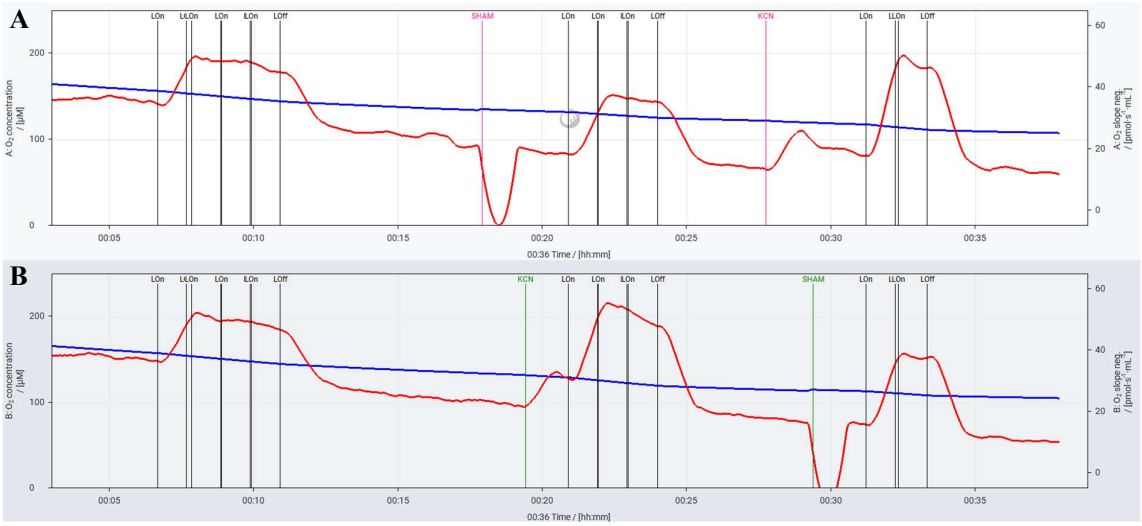

Figure 16: Stimulation of J_D and J_L by KCN but not by SHAM using the internal illumination. For further explanation see Figure 9. (**A**) First titration of SHAM in chamber A and (**B**) first titration of KCN in chamber B.
Experiment: 2023-10-24_Q3-004_02_fresh_prepared_lh.

i) Salicylhydroxamic acid (SHAM): SHAM is an inhibitor of alternative oxidases (AOX) which are present plant mitochondria. SHAM (8 µL 250 mM, Sigma-Aldrich: S607) had no or perhaps a slight stimulatory effect in the presence or absence of KCN (Figure 16). This indicates that the AOX pathway is not involved.

j) Sodium bicarbonate ($NaHCO_3$): 20 µL 5 mM $NaHCO_3$ (Sigma-Aldrich: SX0320) was added in Figure 15 to test if photosynthesis may be activated by bicarbonate. If there is less oxygen consumption after addition of bicarbonate, then this would be evidence for photosynthesis partially compensating for respiration. The decline of J_L over time at 2000 $\mu mol \cdot s^{-1} \cdot m^{-2}$ with two titrations of $NaHCO_3$ was similar to the decline observed in Figure 19. Similarly, no effect of $NaHCO_3$ was apparent on J_D (Figure 17).

Figure 17: No effect of sodium bicarbonate and SHAM on J_D and stimulation by KCN on J_D and J_L using the internal illumination. For further explanation see Figure 9.
Experiment: 2023-10-25_Q3-004_03_fresh_prepared_lh_nahco3 (chamber B).

k) Catalase (Ctl): After adding 5 µL 112000 U/mL Ctl (Sigma-Aldrich: C9322) no catalysing effect to the dismutation of hydrogen peroxide to water and oxygen could be recognized during a light intensity of 2000 $\mu mol \cdot s^{-1} \cdot m^{-2}$ (Figure 18). Therefore, either internal Ctl is saturating or there is no production of H_2O_2.

Figure 18: Experimental plots for CI curves (blue light) and calibration of the internal illumination with light intensities controlled by the PB-Module. Overlay of red and green plots for chamber A and B, respectively. For further explanations see figure 11. Mark a to i correspond to light intensities of 0, 10, 20, 40, 80, 160, 320, 640, 1280, and 2000 µmol·s^{-1}·m^{-2} followed by light intensity 0. PB stop indicates the end of the PB program without change of light intensity. No effect of Ctl.
Experiment: 2023-11-07_Q3-004_02_green_ctl.

l) Ascorbate (As): In the presence of Rot, Ama, and S, 5 µL 800 mM As (Sigma-Aldrich: A7631) was added to obtain a concentration of 2 mM (Figure 19). Rot, Ama, and S exerted no effect on J_D (not shown). As expected, ascorbate increased oxygen consumption due to autoxidation which declined with decreasing c_{O_2}. 2000 µmol·s^{-1}·m^{-2} stimulated J_L to an even larger extent than shown by the uncorrected plot (Figure 19, compare Figure 7B). After reoxygenation autoxidation increased.

m) Chlorophyll-a (Chl-a) a $^1O_2$ producer potentially leading to lipid peroxidation and oxygen consumption, and α-Tocopherol (Toc), an antioxidant of the lipid phase: Chl-a and Toc in the control chamber without lh showed no autoxidation under dark and light conditions (Figure 20, chamber A). Two titrations of Chl-a (1 µL 100µg/mL) and Toc (1µL 1.45 mg/mL) did not prevent the stimulation of oxygen consumption by light (Figure 20, chamber B; Figure 21). Toc was without an effect on J_D (Figure 21). Chl-a was added into chamber B only at 200 µmol·s^{-1}·m^{-2}; the traces remained identical in the two chambers even after increasing the illumination to 2000 µmol·s^{-1}·m^{-2} (Figures 20 and 21).

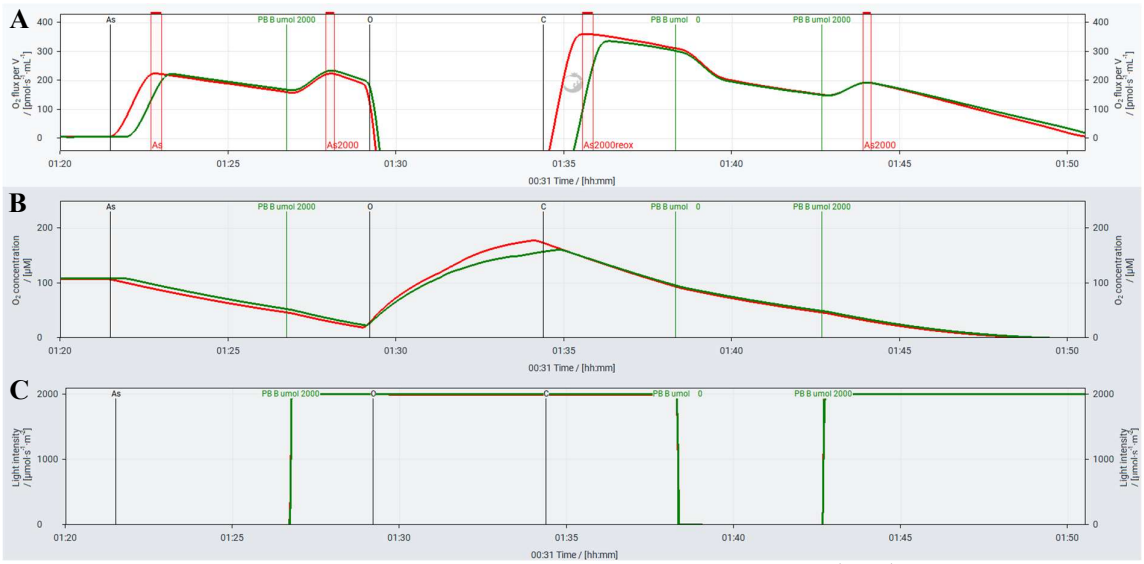

Figure 19: Ascorbate added in the presence of Rot, Ama, and S. (**A**) O_2 flux per V [pmol·s^{-1}·mL^{-1}], (**B**) oxygen concentration [µM], and (**C**) light intensity [µmol·s^{-1}·m^{-2}] plotted as a function of time. For further explanations see Figure 14. The plots are shown after a period of previous measurement.
Experiment: 2023-11-15_Q3-004_06_Ama_rot_S_As.

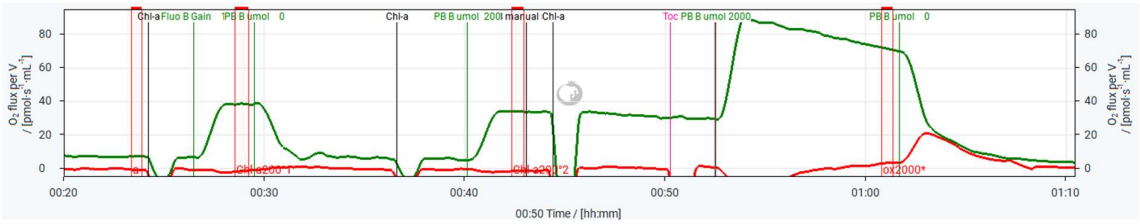

Figure 20: No effect of Chl-a and Toc on the control without lh (chamber A, red plot) and on J_D and J_L in the experiment with lh (chamber B, green plot). For further explanations see Figure 11. Light intensities of 200, 200, and 2000 µmol·s^{-1}·m^{-2}. Note the superimposed plots in the final part of the traces (see Figure x b).
Experiment: 2023-11-23_XA-004_02_chl-a_vs_lh+chl-a.

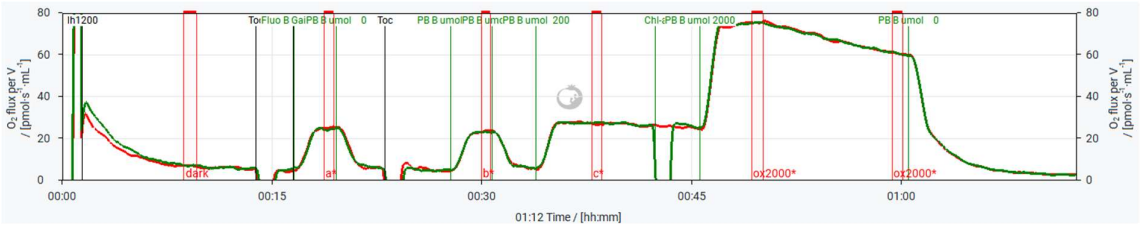

Figure 21: Effect of Toc on lh in chamber A (red plot); effects of Toc and Chl-a on lh in chamber B (green plot). For further explanations see Figure 11. Light intensities of 100, 100, 200, and 2000 µmol·s^{-1}·m^{-2}.
Experiment: 2023-11-23_Q3-004_02_bluelight_toc.

3.5 O_2 consumption-irradiance curves

Instead of a photosynthesis-irradiance (PI) curve in cut leaf pieces (Figure 9), we obtained oxygen consumption-irradiance (CI) curves when there was no measurable photosynthetic activity in leaf homogenates. Light-induced oxygen consumption J_L is calculated as the difference between the total O_2 flux $J_{tot,L}$ measured at any light intensity, corrected for J_D (Figure 22A),

$$J_L = J_{tot,L} - J_D \qquad \text{(Eq. 1)}$$

At the maximum light intensity of 2000 µmol·s^{-1}·m^{-2}, the CI curves reached a plateau in most cases. Therefore, we used J_{2000} as a measure of the maximum light-induced oxygen consumption, $J_{2000} = J_{Lmax}$. Normalized CI curves were obtained by dividing J_L by J_{2000},

$$j_L = J_L / J_{2000} \qquad \text{(Eq. 2)}$$

This yields j_L in the range of 0 to 1 (Figure 22B).

Another normalization relates the values of J_D and J_{2000},

$$j_D = J_D / (J_D + J_{2000}) \qquad \text{(Eq. 3)}$$

Any normalization should avoid a denominator reaching a value of 0 resulting in a non-linear function approaching infinity (Gnaiger, 2020). Theoretically, j_D or J_{2000} may be zero. A range of 0 to 1, therefore, is obtained only by normalizing for $J_D + J_{2000}$. On average, j_D was 0.12 at

the start of the PB program (Tables 3 and 4). In other words, dark oxygen consumption amounted to 12 % of total oxygen consumption measured at 2000 µmol·s^{-1}·m^{-2}.

The total chlorophyll concentration of the fresh and air-dried green leaf homogenate was 54.5 and 80.0 µg/mL (sample 10), respectively. This means the chlorophyll content of the air-dried sample was 47 % higher than in the fresh green samples. Based on the assumption that this difference was entirely due to the lower water content in the air-dried leaf, J_L of the air-dried leaf homogenate was divided by 1.47 as a correction for comparability with J_L of the fresh green leaf homogenates (Figure 22A). This assumption was supported by the similarity of sample 10 (corr.) super imposed with the other CI curves.

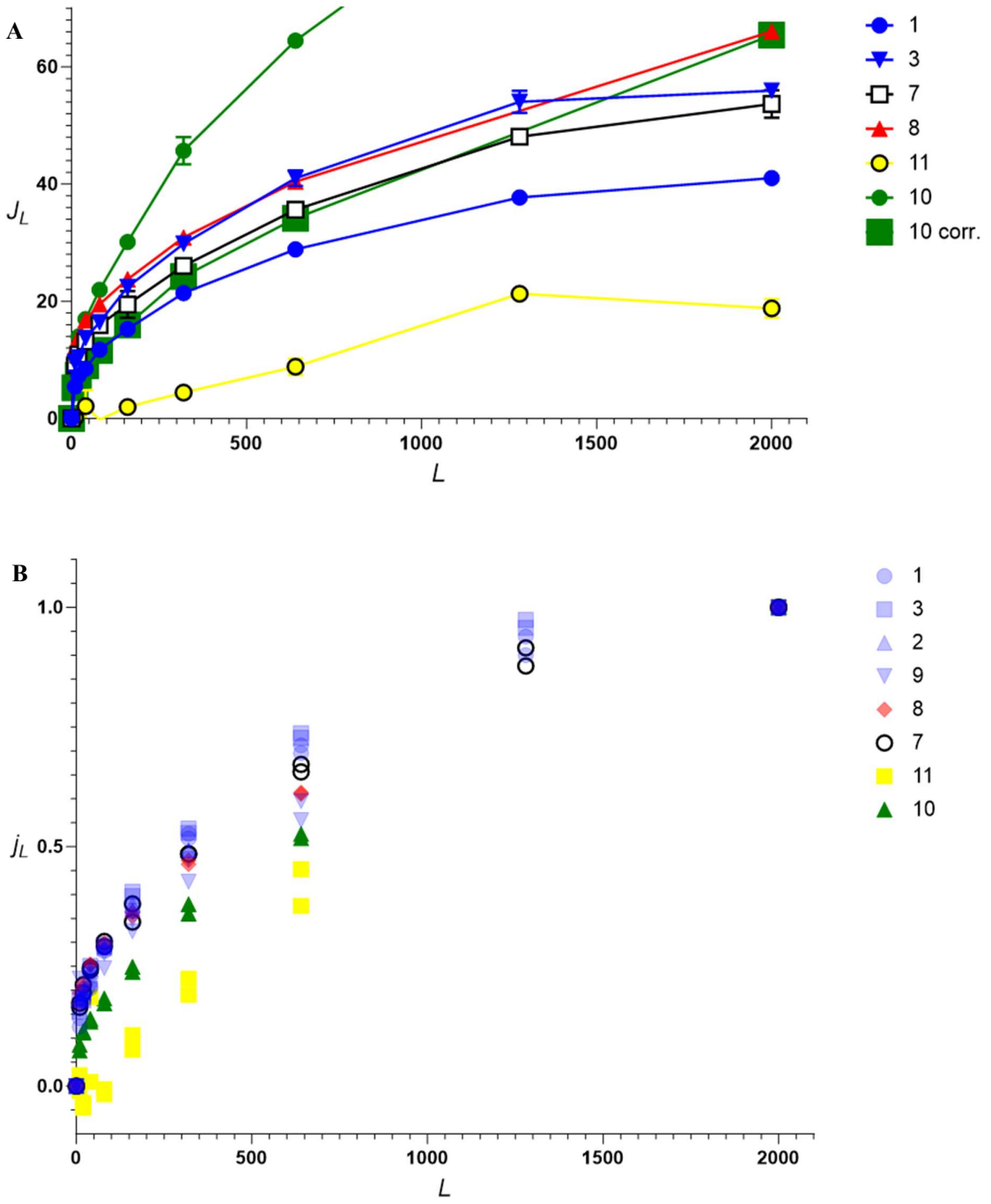

Figure 22: O_2 consumption-irradiance (CI) curves. (**A**) Light-induced oxygen consumption J_L (Eq. 1) as a function of light intensity L [µmol·s^{-1}·m^{-2}]. The three colours of light (BL, samples 1 and 3; WL, sample 7; RL, sample 8) show similar CI curves suggesting that photon-light intensity exerted a predominant effect over energy-light intensity. Fresh yellow leaves samples from the tree are expected to have similar water content compared to fresh green leaves. Therefore, the lower J_L indicates a lower chemical capacity for light-induced oxygen consumption in the yellow leaf (BL, yellow circles, sample 11). In contrast, homogenate from an air-dried green leaf (BL, green circles, sample 10) had a higher J_L than fresh green leaf homogenate. This is expected in terms of a lower water content of the dry leaf. Correction for water content (see text) revealed a CI curve closed to the average of the BL samples 1 and 3 up to 640 µmol·s^{-1}·m^{-2}. Omitting the measurement of 1280 µmol·s^{-1}·m^{-2} might explain a higher J_{2000} in both samples 10 (corr.) and 8. (**B**) CI curves normalized for J_{2000}. The shapes of the CI curves can be compared better by normalization (Eq. 2). The fresh green leaves show similar CI curves independent of light quality (BL, samples 1, 2, 3, and 9; WL, sample 7; RL, sample 8). A right-shift of the CI curve is observed in the dry green leaf (BL, green triangles, sample 10), and this is pronounced further in the fresh yellow leaf (BL, yellow squares, sample 11). At light intensity of 320 µmol·s^{-1}·m^{-2} the right-shift of the CI curve reduced the j_{320} of the fresh yellow leaf to less than 50 % of the green controls. These results support the hypothesis that the photosystem or antenna (i.e. LHC) of the green leaves is responsible for a high efficiency of the absorption of light at low intensity.

3.6 Summary of quantitative results

Date of measurement	2023-11-07		2023-11-08	2023-11-10	2023-11-23	
Sample	**1**	**2**	**3**	**4**	**5** (just B)	**6** (2. thawing)
Time	00:05:22	00:10:27	00:03:14	00:07:17	00:08:46	00:08:42
Blue light A	8.1	19.1	11.9	7.9		7.1
Blue light B	7.1	19.3	11.3	6.3	9.5	7.3
Mean	7.6	19.2	11.6	7.1	9.5	7.2
Sample			**7**			
Time			00:09:05			
White light A			12.2			
White light B			12.1			
Mean			12.2			
Sample				**8**		
Time				00:08:41		
Red light A				8.3		
Red light B				8.2		
Mean				8.3		
Mean all	9.1		SD all		2.1	

Table 2: J_D in different samples of lh. O_2 flux per V of the different samples at the beginning of the measurement without light. Blue, white, and red background colour merely indicate which kind of light was used for the further measurement. Outlined in red is an outlier which was not included in the calculation of the mean of 9.1 pmol·s^{-1}·mL^{-1}.

Technical repeats (chamber A and B with subsamples of the same leaf homogenate) showed high reproducibility (tables 2, 3 and 4). J_D was recorded within 3 to 10 minutes after adding the leaf homogenate into the chamber and marked 'dark' and recorded within 17 to 25 minutes and marked 'a' (Figure 18). The initial dark oxygen flux (3 to 10 minutes) of five different preparations was in the narrow flux range between 7.1 to 12.2 pmol·s^{-1}·mL^{-1} (mean 9.1 ± 2.1 pmol·s^{-1}·mL^{-1}; SD 2.1; N=5; n=2; only n=1 in sample 5), with the exception of sample 2 (19.2 pmol·s^{-1}·mL^{-1}) (Table 2). After 17 to 25 minutes oxygen flux declined to 7.4 ±1.7 pmol·s^{-1}·mL^{-}1 (SD 1.7; N=4; n=2; only n=1 in sample 5) (Table 3). At this time the PB program was started with light intensity changing every 180 seconds from 10, 20, 40, 80, 160, 320, 640, 1280 to 2000 µmol·s^{-1}·m^{-2}. The light-induced oxygen flux was calculated by subtracting from total oxygen flux the value J_D before starting the PB program (Eq. 1). In Table 4 all j_{2000} values are summarized and used for the analysis of their dependence on time and c_{O_2} (Figure 23).

Date of measurement	2023-11-07		2023-11-08	2023-11-10	2023-11-23
Sample	**1**	**2**	**3**	**4***	**5** (just B)
Time	00:24:55	00:21:14	00:17:51	00:17:46	00:23:53
Blue light A	4.9	12.8	7.9	8.5	
Blue light B	4.4	13.4	8.0	7.7	7.3
Mean	4.6	13.1	7.9	8.1	7.3
Sample			**7**		
Time			00:18:26		
White light A			10.6		
White light B			9.0		
Mean			9.8		
Sample				**8**	
Time				00:19:42	
Red light A				6.6	
Red light B				6.7	
Mean				6.6	
Mean all	7.4		SD all	1.7	

Table 3: J_D before the PB program started for recording CI curves. O_2 flux per V of the different samples without light. Blue, white, and red background colour merely indicate which kind of light was used for the further measurement. Outlined in red is an outlier which was not included in the calculations. In sample 4* c, S, $NaHCO_3$ and Azd were added before.

Date of measurement	2023-11-07				2023-11-08				2023-11-10			2023-11-23	
Sample	**1**	**2**			**3**				**4***			**5*** (just B)	**6*** (2. thawing)
Time	01:04:49	01:09:12	01:22:57	01:31:15	00:53:24				00:20:21	00:38:19	01:10:21	01:00:47	00:49:17
O2 concentration A	171	132	103	199	163				236	227	173		177
Blue light A	41.0	68.6	50.3	57.4	56.9				61.6	39.1	54.0		50.2
O2 concentration B	178	128	98	201	165				231	224	171	139	182
Blue light B	41.0	68.5	49.4	56.6	55.0				63.0	41.2	54.7	64.3	51.2
Mean	41.0	68.6	49.9	57.0	55.9				62.3	40.2	54.4	64.3	50.7
Sample					**7**								
Time					00:44:40	01:05:46	01:46:08	02:08:04					
O2 concentration A					155	136	83	239					
White light A					52.0	42.3	22.1	29.2					
O2 concentration B					158	138	84	372					
White light B					55.3	43.1	23.8	34.4					
Mean					53.7	42.7	23.0	31.8					
Sample									**8**				
Time									00:43:21				
O2 concentration A									140				
Red light A									66.4				
O2 concentration B									142				
Red light B									65.8				
Mean									66.1				

Table 4: J_{2000}. O_2 flux per V of the different samples at a final light intensity of 2000 µmol·s^{-1}·m^{-2} of blue, white, or red light indicate by the background colour. Outlined in red is an outlier which was not included in the calculations. In sample 4* c, S, $NaHCO_3$ and Azd, in sample 5* Chl-a, Toc and in sample 6* Toc was added before.

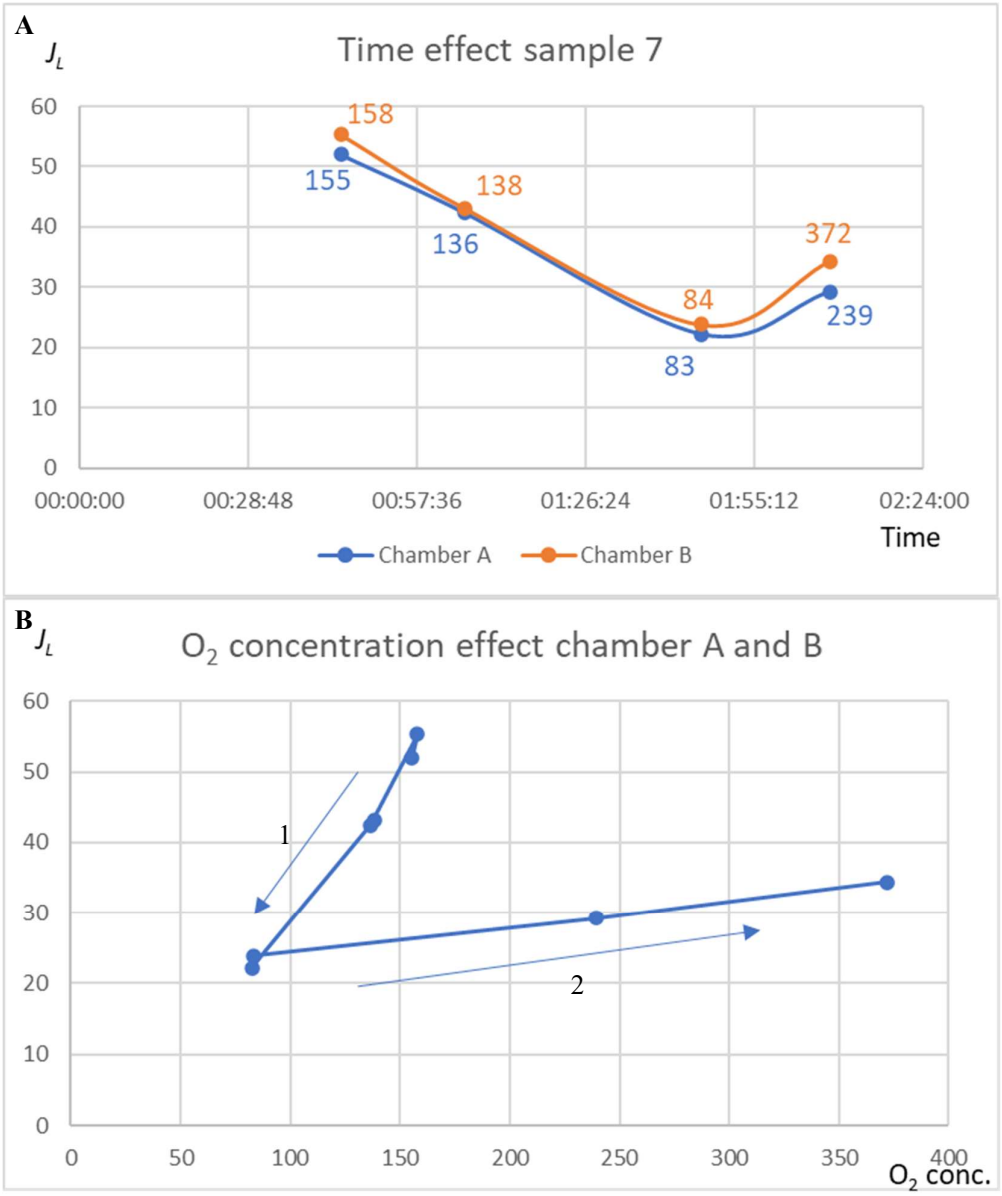

Figure 23: Effect of time and c_{O_2} on J_{2000} in sample 7. (A) Replica of J_{2000} plotted as a function of time at c_{O_2} [µM] indicated by numerals. (B) Replica of J_{2000} plotted as a function of c_{O_2} [µM]. The progression of time is shown by arrows. The decline of c_{O_2} with time is indicated by arrow 1 followed by an increase of c_{O_2} indicated by arrow 2.

3.7 Oxygen kinetics

As shown in Figure 23B, light-induced oxygen consumption was a function of c_{O2} at high concentrations. A detailed analysis of oxygen kinetics was performed by zooming into the low oxygen range below 15 µM where the aerobic-anoxic transition was completed within 15 minutes (Figure 24). J_{2000} declined in a time range of one to two hours, not only as oxygen declined from 160 to 84 µM, but independent of c_{O2} as shown by reoxygenation above air saturation (Figure 23A). Within 15 minutes, however, the time dependence could be assumed to be small. Consequently, the plot of $J_{tot,2000}$ as a function of c_{O2} was interpreted as biphasic oxygen kinetics (Figure 25, plot 1). A linear regression was calculated in the range above 8 µM oxygen, with slope b_{lin} = 1.182 and intercept a_{lin} = 22.8 pmol·s^{-1}·mL^{-1} (plot 2),

$$J_{2000(lin)} = b_{lin} \cdot c_{O2} + a_{lin} \qquad \text{(Eq. plot 2)}$$

The linear contribution to oxygen kinetics J_{lin}, therefore, is described by Eq. plot 2 moved to the origin, with a'_{lin} = 0 pmol·s^{-1}·mL^{-1} and b_{lin} = 1.182 (plot 3),

$$J_{lin} = b_{lin} \cdot c_{O2} \qquad \text{(Eq. plot 3)}$$

The remaining kinetic contribution is then defined as plot 1 minus plot 3, obtaining the data in plot 4 (Figure 25). Plots 1 and 4 decline theoretically to zero flux at zero oxygen concentration. However, a small oxygen backdiffusion a^0 = -2.1 pmol·s^{-1}·mL^{-1} (Figure 6) is compensated by oxygen consumption when approaching a steady state close to anoxia (Figure 24) (Gnaiger *et al.*, 1995; Gnaiger, 2001). Plot 4 followed a monophasic hyperbolic function J_{hyp} with intercept $-a^0$ = 2.1 pmol·s^{-1}·mL^{-1}. The maximum flux of the hyperbolic part $J_{hyp,max}$ is defined by the intercept b_{lin} of the linear contribution (Eq. plot 2), i.e. $J_{hyp,max}$ = 22.8 pmol·s^{-1}·mL^{-1},

$$J_{hyp} = -a^0 + (J_{hyp,max} \cdot c_{O2}) / (c_{50} + c_{O2}) \qquad \text{(Eq. plot 4)}$$

In nonlinear regression analysis (Eq. plot 4), therefore, $J_{hyp,max} = b_{lin}$ was inserted as a constant and only the oxygen concentration at half-maximal flux, c_{50}, was fitted as a parameter, obtaining c_{50} = 0.9 µM (Figure 25).

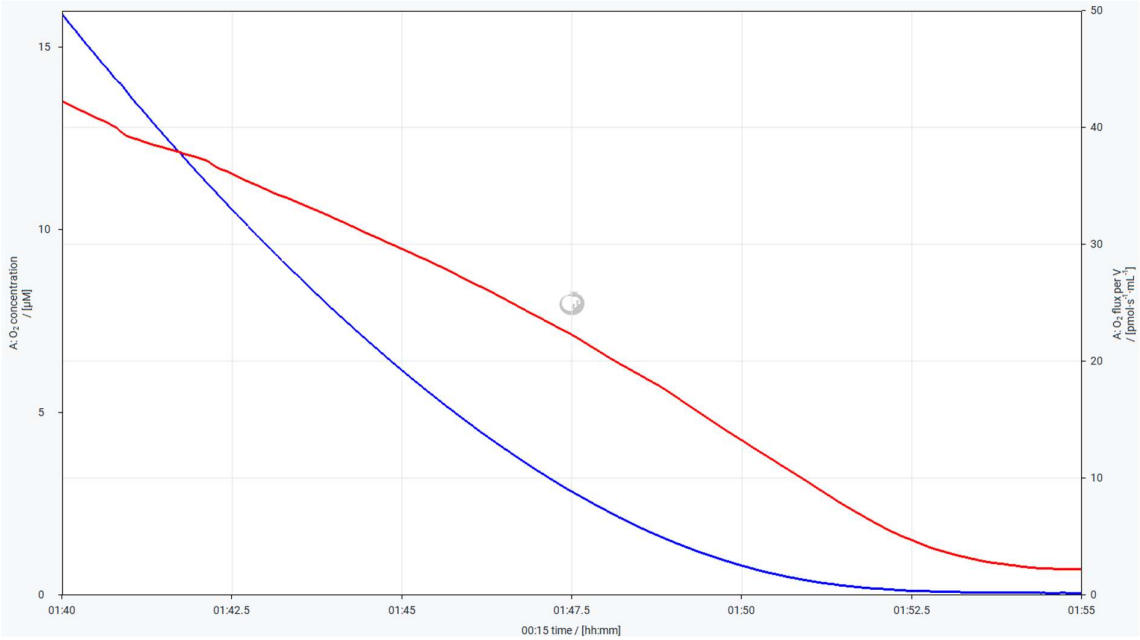

Figure 24: Traces of $J_{tot,2000}$ (red plot) and c_{O2} (blue plot) as a function of time in the section of aerobic-anoxic transition use for oxygen kinetic analysis (Figure 24). Zoom into the hypoxic range of 16 to 0 µM.
Experiment: 2023-11-10_XA-002_03_O2kinetik_R0.

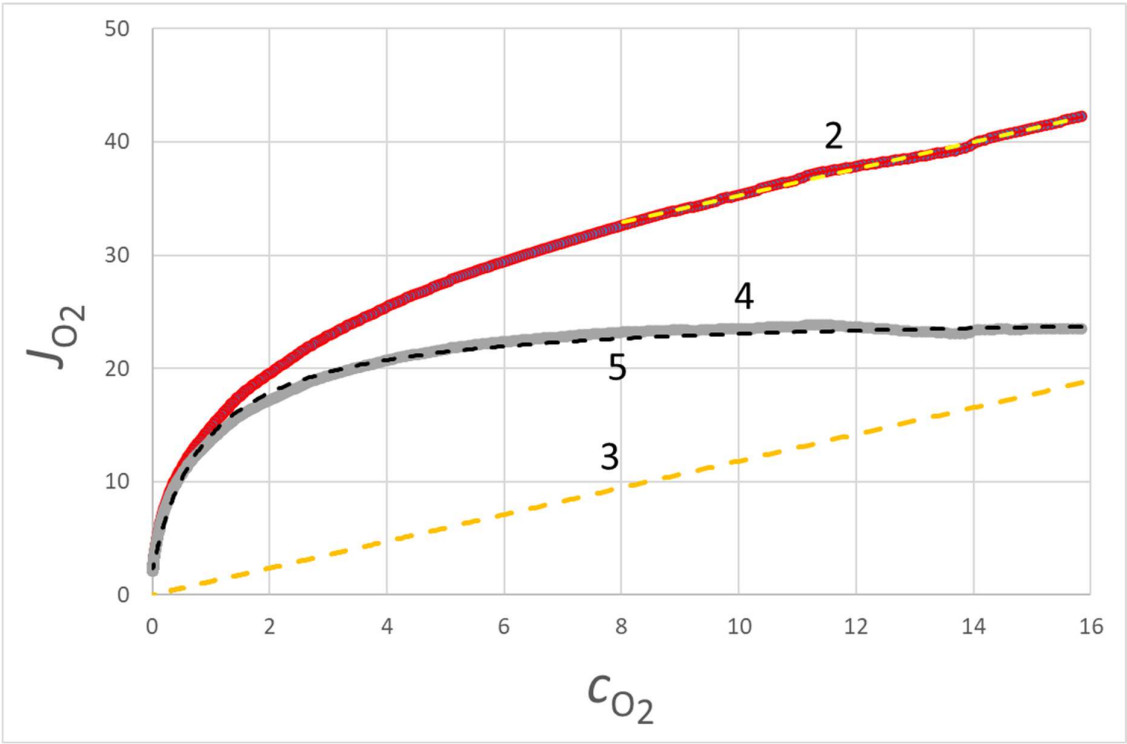

Figure 25: Biphasic oxygen kinetics of $J_{tot,2000}$. Plot 1 (red): Measured $J_{tot,2000}$ as a function of c_{O_2}. Plot 2: Linear part of $J_{tot,2000}$ with linear regression (yellow dashed line, Eq. plot 2). Plot 3: Linear regression with zero intercept (dashed line, Eq. plot 3). Plot 4 (grey): Hyperbolic component of oxygen kinetics calculated as plot 1 minus plot 3. Plot 5 (dashed line): Hyperbolic regression line (Eq. plot 5).

4 Discussion

Photodecomposition and oxygen consumption irradiance (CI) curves emerged as the most important topics of the present study. Photodecomposition is an important process in forest ecosystems, directly linked to current issues of global carbon balance and changing environmental stress factors impacting leaf degradation (King, Brandt and Adair, 2012; Pieristè *et al.*, 2019; Wang *et al.*, 2021; Hussain *et al.*, 2023).

In the face of escalating air pollution, climate change, and their interconnected impacts on forest ecosystems, the role of finding new indicators by modern research cannot be overstated. It remains a challenge to develop tools to unravel the complexity of interactions between trees and various stressors, offering guidelines for conservation and sustainable management. As we navigate the challenges posed by environmental pressures, improved indicators will guide us towards a more comprehensive understanding of the intricate dynamics within forest ecosystems.

The shape of PI curves may be compared to the CI curves obtained in the present study. The CI curves for different light qualities (BL, WL, and RL) suggest that photon-light intensity plays a predominant role in influencing J_L. This implies that the photon-intensity of light source has a consistent impact on the processes responsible for oxygen consumption, irrespective of the spectral composition. The right-shift observed in the dry green leaf and further pronounced in the fresh yellow leaf suggests altered efficiency. Notably, at a light intensity of 320 $\mu mol \cdot s^{-1} \cdot m^{-2}$, the right-shift reduced J_L in the fresh yellow leaf to less than 50 % of the green controls. This substantial reduction in J_L supports the hypothesis that the photodecomposition in green leaves is highly efficient in light absorption at low intensities.

A novel finding was the biphasic oxygen kinetics of light-induced oxygen consumption. A hyperbolic oxygen kinetics indicates a saturation mechanism with involvement of enzymatic catalysis. The high oxygen affinity of this process as expressed by the extremely low c_{50} below 1 µM O_2 supports the involvement of an enzyme-catalysed process. A c_{50} below 1 µM O_2 is characteristic of mitochondrial respiration (Gnaiger *et al.*, 1995; Scandurra and Gnaiger, 2010; Harrison *et al.*, 2015). It remains to be investigated, if application of specific inhibitors of chloroplast electron transfer (e.g. DCMU) exert any effect on the c_{50} of light-induced oxygen consumption in the leaf homogenates. The linear oxygen kinetics of autoxidation and hydrogen peroxide production extends into the hyperoxic range (Boveris and Chance, 1973; Gnaiger *et al.*, 1995; Hütter *et al.*, 2002; Komlódi, Sobotka and Gnaiger, 2021) which is

consistent with the biphasic dependence of light-induced oxygen consumption on oxygen concentration observed in the present study.

Sample collection for studying the leaves of trees (in this study *Robinia pseudoacacia*) requires key considerations including strategic tree selection, standardized sampling locations from various parts of the tree, immediate and consistent sample processing, standardized homogenization techniques, and controlled drying protocols to simulate drought, temporal diversity in sampling. Inherent limitations in this study regarding such requirements remain to be addressed in future investigations.

By examining leaves as early indicators, researchers gain insights into the health and functioning of trees at a crucial stage. Monitoring oxygen dynamics in leaves provides a window into the intricate web of interactions between trees and environmental stressors. As we strive for a deeper understanding of the challenges faced by forests, the focus on leaves and their physiological processes offers a promising avenue for developing effective and timely conservation strategies. In essence, the exploration of early indicators within easily accessible compartments, such as leaves, serves as a vital step towards enhancing our ability to protect and sustain forest ecosystems in the face of ongoing environmental changes.

5 Conclusion

The quest for developing early indicators of environmental impacts on forest management in the face of escalating threats to forest ecosystems underscores the significance of focusing on easily accessible compartments of trees. Leaves emerge as a pivotal target in this endeavor, given their crucial role in energy supply. Whereas the importance of leaves is well established in the context of photosynthesis and cellular respiration, leaf decomposition becomes increasingly recognized as a key process in global carbon balance. Inhibitor titrations ruling out a mitochondrial contribution to dark and light-induced oxygen consumption indicate that mitochondrial electron transfer was not damaged by high light intensity but had become dysfunctional during homogenization. The high reproducibility observed in the technical repeats underscores the reliability and consistency of the measurement of the oxygen consumption by high-resolution respirometry. Measurement of the dependence of photodecomposition on light intensity (CI curves) and the oxygen dependence of photodecomposition present a novel approach enabled by implementation of controlled light intensity in advanced high-resolution respirometry.

List of literature

Air calibration - Bioblast (no date). Available at: https://wiki.oroboros.at/index.php/Air_calibration (Accessed: 26 December 2023).

ALAS – Universität Innsbruck (no date). Available at: https://www.uibk.ac.at/de/botany/forschung/projekte/alas/ (Accessed: 26 December 2023).

Baglivo, E. *et al.* (2022) 'Statistical analysis of instrumental reproducibility as internal quality control in high-resolution respirometry', *Bioenergetics Communications*, 2022, pp. 8–8. Available at: https://doi.org/10.26124/bec:2022-0008.

Barreto, P. *et al.* (2022) 'Metabolism and Signaling of Plant Mitochondria in Adaptation to Environmental Stresses', *International Journal of Molecular Sciences*, 23(19). Available at: https://doi.org/10.3390/ijms231911176.

Boveris, A. and Chance, B. (1973) 'The mitochondrial generation of hydrogen peroxide. General properties and effect of hyperbaric oxygen', *The Biochemical Journal*, 134(3), pp. 707–716. Available at: https://doi.org/10.1042/bj1340707.

Flux - Bioblast (no date). Available at: https://wiki.oroboros.at/index.php/Flux (Accessed: 26 December 2023).

Flux / Slope - Bioblast (no date). Available at: https://wiki.oroboros.at/index.php/Flux_/_Slope (Accessed: 26 December 2023).

Gnaiger, E. (1983) 'Heat dissipation and energetic efficiency in animal anoxibiosis: Economy contra power', *Journal of Experimental Zoology*, 228(3), pp. 471–490. Available at: https://doi.org/10.1002/jez.1402280308.

Gnaiger, E. *et al.* (1995) 'Control of mitochondrial and cellular respiration by oxygen', *Journal of Bioenergetics and Biomembranes*, 27(6), pp. 583–596. Available at: https://doi.org/10.1007/BF02111656.

Gnaiger, E. (2001) 'Bioenergetics at low oxygen: dependence of respiration and phosphorylation on oxygen and adenosine diphosphate supply', *Respiration Physiology*, 128(3), pp. 277–297. Available at: https://doi.org/10.1016/S0034-5687(01)00307-3.

Gnaiger, E. (2020) 'Mitochondrial Pathways and Respiratory Control: An Introduction to OXPHOS Analysis. 5th ed.' Available at: https://doi.org/10.26124/BEC:2020-0002.

Gnaiger, E. *et al.* (2020) 'Mitochondrial physiology'. Available at: https://doi.org/10.26124/BEC:2020-0001.V1.

Gnaiger, E. *et al.* (2023) 'MiPNet22.11_O2k-FluoRespirometer-manual'. Available at: https://wiki.oroboros.at/images/2/29/MiPNet22.11_O2k-FluoRespirometer-manual.pdf.

Gull, A. *et al.* (2019) 'Biotic and Abiotic Stresses in Plants', in *Abiotic and Biotic Stress in Plants*. IntechOpen. Available at: https://doi.org/10.5772/intechopen.85832.

Harrison, D.K. *et al.* (2015) 'Cytochrome redox states and respiratory control in mouse and beef heart mitochondria at steady-state levels of hypoxia', *Journal of Applied Physiology (Bethesda, Md.: 1985)*, 119(10), pp. 1210–1218. Available at: https://doi.org/10.1152/japplphysiol.00146.2015.

Hussain, M.B. *et al.* (2023) 'Photodegradation and Its Effect on Plant Litter Decomposition in Terrestrial Ecosystems: A Systematic Review', *Soil Systems*, 7(1), p. 6. Available at: https://doi.org/10.3390/soilsystems7010006.

Hütter, E. *et al.* (2002) 'Biphasic oxygen kinetics of cellular respiration and linear oxygen dependence of antimycin A inhibited oxygen consumption', *Molecular Biology Reports*, 29(1–2), pp. 83–87. Available at: https://doi.org/10.1023/a:1020322922732.

King, J.Y., Brandt, L.A. and Adair, E.C. (2012) 'Shedding light on plant litter decomposition: advances, implications and new directions in understanding the role of photodegradation', *Biogeochemistry*, 111(1), pp. 57–81. Available at: https://doi.org/10.1007/s10533-012-9737-9.

Klughammer, C. and Schreiber, U. (2008) 'Complementary PS II quantum yields calculated from simple fluorescence parameters measured by PAM fluorometry and the Saturation Pulse method'.

Komlódi, T., Sobotka, O. and Gnaiger, E. (2021) 'Facts and artefacts on the oxygen dependence of hydrogen peroxide production using Amplex UltraRed'. Available at: https://doi.org/10.26124/MITOFIT:2021-0010.

Laisk, A. and Oja, V. (2018) 'Kinetics of photosystem II electron transport: a mathematical analysis based on chlorophyll fluorescence induction', *Photosynthesis Research*, 136(1), pp. 63–82. Available at: https://doi.org/10.1007/s11120-017-0439-y.

Liebig, J. von (1842) *Die organische Chemie in ihrer Anwendung auf Physiologie und Pathologie*. 1. Auflage. Braunschweig: Vieweg.

Lusk, G. (1928) *The elements of the science of nutrition*. 4th ed., reset. Philadelphia and London: W.B. Saunders Company.

Maliga, P. (2014) *Chloroplast Biotechnology: Methods and Protocols*. Available at: https://doi.org/10.1007/978-1-62703-995-6.

Meszaros, A.T. *et al.* (2022) 'Mitochondrial respiration during normothermic liver machine perfusion predicts clinical outcome', *EBioMedicine*, 85, p. 104311. Available at: https://doi.org/10.1016/j.ebiom.2022.104311.

MiR05-Kit (no date) *Oroboros Instruments*. Available at: https://www.oroboros.at/index.php/product/mir05-kit/ (Accessed: 26 December 2023).

MitoPedia - Bioblast (no date). Available at: https://www.bioblast.at/index.php/MitoPedia#MitoPedia:_MiP_and_biochemistry (Accessed: 11 January 2024).

MitoPedia: DatLab - Bioblast (no date). Available at: https://wiki.oroboros.at/index.php/MitoPedia:_DatLab (Accessed: 26 December 2023).

PB Light Source - Bioblast (no date). Available at: https://wiki.oroboros.at/index.php/PB_Light_Source (Accessed: 26 December 2023).

PB-Module - Bioblast (no date). Available at: https://wiki.oroboros.at/index.php/PB-Module (Accessed: 26 December 2023).

Petrović, S., Zvezdanović, J. and Marković, D. (2017) 'Chlorophyll degradation in aqueous mediums induced by light and UV-B irradiation: An UHPLC-ESI-MS study', *Radiation Physics and Chemistry*, 141, pp. 8–16. Available at: https://doi.org/10.1016/j.radphyschem.2017.05.024.

Pfanz, H. and Heber, U. (1986) 'Buffer Capacities of Leaves, Leaf Cells, and Leaf Cell Organelles in Relation to Fluxes of Potentially Acidic Gases 1', *Plant Physiology*, 81(2), pp. 597–602.

Piechulla, B. and Heldt, H.W. (2023) *Pflanzenbiochemie*. Berlin, Heidelberg: Springer. Available at: https://doi.org/10.1007/978-3-662-65429-3.

Pieristè, M. *et al.* (2019) 'Solar UV-A radiation and blue light enhance tree leaf litter decomposition in a temperate forest', *Oecologia*, 191(1), pp. 191–203. Available at: https://doi.org/10.1007/s00442-019-04478-x.

Polle, A. and Rennenberg, H. (2019) *Physiological Responses to Abiotic and Biotic Stress in Forest Trees*. MDPI - Multidisciplinary Digital Publishing Institute.

Porra, R.J., Thompson, W.A. and Kriedemann, P.E. (1989) 'Determination of accurate extinction coefficients and simultaneous equations for assaying chlorophylls a and b extracted with four different solvents: verification of the concentration of chlorophyll standards by atomic absorption spectroscopy', *Biochimica et Biophysica Acta (BBA) - Bioenergetics*, 975(3), pp. 384–394. Available at: https://doi.org/10.1016/S0005-2728(89)80347-0.

Potočić, N. (2023) 'Advances in Forest Ecophysiology: Stress Response and Ecophysiological Indicators of Tree Vitality', *Plants*, 12(5), p. 1063. Available at: https://doi.org/10.3390/plants12051063.

Roach, T. *et al.* (2018) 'Distress and eustress of reactive electrophiles and relevance to light stress acclimation via stimulation of thiol/disulphide-based redox defences', *Free Radical Biology and Medicine*, 122, pp. 65–73. Available at: https://doi.org/10.1016/j.freeradbiomed.2018.03.030.

Roach, T. (2022) ‘Chlorophyll fluorescence of Chlamydomonas reinhardtii: insights into the complexities’, *Bioenergetics Communications*, 2022, pp. 10–10. Available at: https://doi.org/10.26124/bec:2022-0010.

Roach, T. *et al.* (2023) ‘Heat Acclimation under Drought Stress Induces Antioxidant Enzyme Activity in the Alpine Plant Primula minima’, *Antioxidants*, 12(5), p. 1093. Available at: https://doi.org/10.3390/antiox12051093.

Roach, T. and Krieger-Liszkay, A. (2019) ‘Photosynthetic Regulatory Mechanisms for Efficiency and Prevention of Photo-Oxidative Stress’, in *Annual Plant Reviews online*. John Wiley & Sons, Ltd, pp. 273–306. Available at: https://doi.org/10.1002/9781119312994.apr0666.

Ruban, A.V. (2016) ‘Nonphotochemical Chlorophyll Fluorescence Quenching: Mechanism and Effectiveness in Protecting Plants from Photodamage1’, *Plant Physiology*, 170(4), pp. 1903–1916. Available at: https://doi.org/10.1104/pp.15.01935.

Sample type - Bioblast (no date). Available at: https://wiki.oroboros.at/index.php/Sample_type (Accessed: 9 December 2023).

Scandurra, F.M. and Gnaiger, E. (2010) ‘Cell Respiration Under Hypoxia: Facts and Artefacts in Mitochondrial Oxygen Kinetics’, in E. Takahashi and D.F. Bruley (eds) *Oxygen Transport to Tissue XXXI*. Boston, MA: Springer US (Advances in Experimental Medicine and Biology), pp. 7–25. Available at: https://doi.org/10.1007/978-1-4419-1241-1_2.

Schmitz, J. (2011) *Untersuchungen zur Hochlicht-Akklimatisierung von Arabidopsis thaliana Mutanten mit Defekten im Kohlenhydratstoffwechsel*. text.thesis.doctoral. Universität zu Köln. Available at: http://www.uni-koeln.de/ (Accessed: 26 December 2023).

Schwarzländer, M. and Finkemeier, I. (2013) ‘Mitochondrial Energy and Redox Signaling in Plants’, *Antioxidants & Redox Signaling*, 18(16), pp. 2122–2144. Available at: https://doi.org/10.1089/ars.2012.5104.

Shimakawa, G., Kohara, A. and Miyake, C. (2021) 'Characterization of Light-Enhanced Respiration in Cyanobacteria', *International Journal of Molecular Sciences*, 22(1), p. 342. Available at: https://doi.org/10.3390/ijms22010342.

Shimakawa, G., Krieger-Liszkay, A. and Roach, T. (2022) 'ROS-derived lipid peroxidation is prevented in barley leaves during senescence', *Physiologia Plantarum*, 174(5), p. e13769. Available at: https://doi.org/10.1111/ppl.13769.

Stirrer test - Bioblast (no date). Available at: https://wiki.oroboros.at/index.php/Stirrer_test (Accessed: 26 December 2023).

Taylor, N.L. (ed.) (2019) *Plant Mitochondria*. MDPI - Multidisciplinary Digital Publishing Institute. Available at: https://doi.org/10.3390/books978-3-03897-551-9.

Vera-Vives, A.M.V., Perin, G. and Morosinotto, T. (2022) 'High-resolution photosynthesis-irradiance curves in microalgae', *Bioenergetics Communications*, 2022, pp. 19–19. Available at: https://doi.org/10.26124/bec:2022-0019.

Wang, Q. *et al.* (2021) 'The contribution of photodegradation to litter decomposition in a temperate forest gap and understorey', *The New Phytologist*, 229(5), pp. 2625–2636. Available at: https://doi.org/10.1111/nph.17022.

Went, N. *et al.* (2022) 'Oxygen dependence of photosynthesis and light-enhanced dark respiration studied by high-resolution PhotoRespirometry', *Biochimica et Biophysica Acta (BBA) - Bioenergetics*, 1863, p. 148832. Available at: https://doi.org/10.1016/j.bbabio.2022.148832.

Wetter und Klima - Deutscher Wetterdienst - Thema des Tages - Die Sonne machte 2022 Überstunden - Endbilanz (no date). Available at: https://www.dwd.de/DE/wetter/thema_des_tages/2023/1/14.html (Accessed: 26 December 2023).

Zero calibration - Bioblast (no date). Available at: https://wiki.oroboros.at/index.php/Zero_calibration (Accessed: 26 December 2023).

List of figures

List of tables

Abstract

This study presents a novel approach to measure oxygen consumption and production under controlled light conditions in preparations of leaf samples using the Oroboros O2k high-resolution respirometer. Dark respiration, photosynthesis-irradiance (PI) curves, and photodegradation described by oxygen consumption-irradiance (CI) curves were obtained accurately and reproducibly on leaf preparations. The developed protocols for high-resolution respirometry and photobiology provide a novel approach for understanding plant respiratory and photosynthetic processes.

Green and yellow senescent leaves were collected from a *Robinia pseudoacacia* tree in the fall. The sample preparation involved the cutting and homogenization of leaves in two different media. Fresh and frozen samples of leaf homogenate were compared. First experimental test series are reported using the O2k equipped with the PhotoBiology (PB) Module. The instrument was controlled by, and data were recorded with DatLab 8, and the obtained data were further analyzed with Excel and GraphPad.

Dark respiration and photosynthetic activity of cut leaf pieces were plotted as a function of light intensity to obtain photosynthesis-irradiance (PI) curves in the range of light intensities of 10 to 2000 $\mu mol \cdot s^{-1} \cdot m^{-2}$. Measurements of oxygen consumption in the dark and at different light intensities revealed in the leaf homogenates an unexpected increase of oxygen consumption with blue, red, and white light. Mirror images of PI curves were remarkably similar to the shape of oxygen consumption-irradiance (CI) curves.

Mitochondrial dark respiration and chloroplast photorespiration are superimposed by residual oxygen consumption (*Rox)*, defined as the oxygen consumption due to oxidative side reactions remaining after inhibition of the mitochondrial and chloroplast electron transfer pathways to oxygen. Application of selective inhibitors of the mitochondrial electron transfer system provided evidence against the involvement of mitochondrial electron transfer in dark and light-induced oxygen consumption of the leaf homogenates which, therefore, was characterized as photodegradation. The effect of inhibitors of the chloroplast electron transfer system on photodegradation remains to be investigated.

Further studies are required with leaves at different stages of their life cycle and with sample preparations which preserve the functional integrity of mitochondria and chloroplasts. The production of reactive oxygen species is probably involved in photodegradation, which is an ecologically relevant process in various stages of the lifecycle of leaves and becomes

progressively or abruptly dominant towards the final phase of leaf decomposition. Integrating this perspective into studies of dark respiration and photosynthesis of different species is an entirely new application field of high-resolution respirometry. It has a great potential to advance our understanding of plant physiology and analysis of the carbon balance in forest ecosystems and agriculture.